© 2014. Published by The Company of Biologists Ltd | Development (2014) 141, 1416 doi:10.1242/dev.108803

CORRECTION

Reconstruction of phrenic neuron identity in embryonic stem cell-derived motor neurons

Carolina Barcellos Machado, Kevin C. Kanning, Patricia Kreis, Danielle Stevenson, Martin Crossley, Magdalena Nowak, Michelina Iacovino, Michael Kyba, David Chambers, Eric Blanc and Ivo Lieberam

There was an error published in *Development* **141**, 784-794.

In the supplementary data originally published, the supplementary Materials and methods section was missing. The correct version now appears online.

We apologise to the authors and readers for this mistake.

© 2014. Published by The Company of Biologists Ltd | Development (2014) 141, 784-794 doi:10.1242/dev.097188

RESEARCH ARTICLE

STEM CELLS AND REGENERATION

Reconstruction of phrenic neuron identity in embryonic stem cell-derived motor neurons

Carolina Barcellos Machado[1,*], Kevin C. Kanning[2], Patricia Kreis[1], Danielle Stevenson[1], Martin Crossley[1], Magdalena Nowak[1], Michelina Iacovino[3], Michael Kyba[3], David Chambers[1], Eric Blanc[1] and Ivo Lieberam[1,*]

ABSTRACT

Air breathing is an essential motor function for vertebrates living on land. The rhythm that drives breathing is generated within the central nervous system and relayed via specialised subsets of spinal motor neurons to muscles that regulate lung volume. In mammals, a key respiratory muscle is the diaphragm, which is innervated by motor neurons in the phrenic nucleus. Remarkably, relatively little is known about how this crucial subtype of motor neuron is generated during embryogenesis. Here, we used direct differentiation of motor neurons from mouse embryonic stem cells as a tool to identify genes that direct phrenic neuron identity. We find that three determinants, Pou3f1, Hoxa5 and Notch, act in combination to promote a phrenic neuron molecular identity. We show that Notch signalling induces Pou3f1 in developing motor neurons *in vitro* and *in vivo*. This suggests that the phrenic neuron lineage is established through a local source of Notch ligand at mid-cervical levels. Furthermore, we find that the cadherins Pcdh10, which is regulated by Pou3f1 and Hoxa5, and Cdh10, which is controlled by Pou3f1, are both mediators of like-like clustering of motor neuron cell bodies. This specific Pcdh10/Cdh10 activity might provide the means by which phrenic neurons are assembled into a distinct nucleus. Our study provides a framework for understanding how phrenic neuron identity is conferred and will help to generate this rare and inaccessible yet vital neuronal subtype directly from pluripotent stem cells, thus facilitating subsequent functional investigations.

KEY WORDS: Embryonic stem cell, Phrenic neuron, Transcriptional identity, Motor neuron differentiation

INTRODUCTION

Land vertebrates, including humans, use lungs to breathe air. The inspiratory and expiratory movements of the lungs are driven by a complex neural circuitry that consists of a central network in the brainstem that generates breathing rhythms and an output layer of motor neurons (MNs) that connect to respiratory muscles. These respiratory circuits develop prenatally and must become functional immediately after birth. Although significant progress has been made in understanding the central pattern generator itself (Champagnat et al., 2009; Fortin and Thoby-Brisson, 2009), relatively little is known about the formation of MNs that relay breathing rhythms from the CNS to the periphery. In mammals, respiration is driven by muscles that connect to the rib cage and thereby indirectly inflate and deflate the lungs. Arguably, the most important of these muscles is the diaphragm, which forms the boundary between the thoracic and abdominal cavities and contracts during inspiration. The diaphragm is innervated by the phrenic nucleus (PN), a population of MNs located in the mid-cervical spinal cord. During embryonic development, phrenic neurons emerge alongside other MNs from ventral progenitors (Arber et al., 1999; Briscoe et al., 2000; Thaler et al., 1999), send their axons through cervical ventral roots and then project caudally through the thoracic cavity to innervate the diaphragm muscle (Allan and Greer, 1997). We have only a partial understanding of the molecular cascade that establishes phrenic MN identity. It is, however, important that this pathway is defined as this would provide insights into how mammal-specific anatomical adaptations are patterned and allow us to model aspects of respiratory motor circuitry in neuronal cultures to study neuromuscular function and disease.

Spinal MNs segregate into distinct columns during embryogenesis. Each column connects to a specific set of muscles: the medial motor column (MMC) projects to epaxial muscles, the lateral motor column (LMC) innervates limb muscles (Lance-Jones and Landmesser, 1980; Tsuchida et al., 1994), and the hypaxial motor column (HMC) innervates body wall muscles (Dasen et al., 2003; Peljto and Wichterle, 2011). MNs acquire subtype transcriptional identities due to exposure to locally restricted morphogens (Marshall et al., 1992). For example, the expression of the MMC determinants Lhx3 and Lhx4 is sustained by floor plate-derived Wnt4 and Wnt5 (Agalliu et al., 2009). Likewise, brachial LMC fate depends on overlapping, segmentally restricted gradients of retinoic acid and Fgfs (Liu et al., 2001), which induce Hox6 paralogues and the accessory factor Foxp1 in presumptive LMC neurons in register with forelimbs (Dasen et al., 2008; Dasen et al., 2003). The HMC, by contrast, appears to lack specific determinants and might represent a ground state of MNs. Phrenic neurons are thought to be derivatives of the HMC (Rousso et al., 2008).

Some candidate determinants for early phrenic development have been identified, although their contribution to phrenic neuron specification is poorly understood: the transcription factor (TF) Pou3f1 is enriched in phrenic neurons, and *Pou3f1* deficiency in mice leads to disorganisation of the PN (Bermingham et al., 1996). Absence of mid-cervical Hox5 paralogues affects the maintenance of phrenic neurons, but not their initial specification (Philippidou et al., 2012). Lastly, Foxp1 appears to negatively regulate the phrenic MN lineage, since *Foxp1* mutants have increased numbers of phrenic MNs (Rousso et al., 2008). What is largely lacking at this point is an understanding of which potential effector genes are downstream of these factors, how these and other determinants interact and, in the case of Pou3f1, how the expression of the factor itself is initiated.

[1]MRC Centre for Developmental Neurobiology, King's College London, London SE1 1UL, UK. [2]Motor Neuron Center, Columbia University, New York, NY 10032, USA. [3]Lillehei Heart Institute, University of Minnesota, Minneapolis, MN 55455, USA.

*Authors for correspondence (carolina.barcellos_machado@kcl.ac.uk; ivo.lieberam@kcl.ac.uk)

Received 16 April 2013; Accepted 20 November 2013

Development (2014) doi:10.1242/dev.097188

MN development can be recapitulated *in vitro* from mouse or human embryonic stem cells (ESCs), which will form functional spinal MNs under the appropriate culture conditions (Li et al., 2008; Miles et al., 2004; Wichterle et al., 2002). ESC-derivation of MNs depends on the same extrinsic and intrinsic cues that act during normal embryogenesis and has been repeatedly used to investigate subtype-specific developmental pathways in these cells (Jung et al., 2010; Peljto et al., 2010; Soundararajan et al., 2006). We set out to apply this approach to the acquisition of phrenic neuron identity.

To address how phrenic neuron fate is established in the developing spinal cord, we first identified candidate determinants in primary MNs sorted from mouse embryos, and then used a systematic *in vitro* gain-of-function (GOF) screening approach to test whether any given candidate approximates phrenic neuron transcriptional patterns when ectopically expressed in ESC-derived MNs (ESC-MNs). The aim was to define modules of effector genes downstream of the key determinants, as well as to understand how the determinants interact with each other. We found that the TFs Pou3f1, Hoxa5 and Notch intracellular domain (NICD) combine to regulate distinct sets of effector genes, which together comprise a large fraction of all phrenic neuron-specific genes. Moreover, expression of the receptors Cdh10, which is downstream of Pou3f1, or Pcdh10, a gene coordinately regulated by Hoxa5 and Pou3f1, is sufficient to mediate like-like clustering of MNs into aggregates *in vitro*, mimicking nucleus formation *in vivo*. Our findings suggest that local Notch-Delta interaction in the ventral spinal cord might be an early event in phrenic neuron specification and that a defined combination of intrinsic and/or extrinsic factors may be used to emulate phrenic neuron transcriptional identity and morphological features in MNs derived from pluripotent stem cells *in vitro*.

RESULTS

Isolation of phrenic neurons from E11.5 mouse embryos by flow cytometry

In the ventral embryonic spinal cord, phrenic neurons are generated alongside other MNs from ventral progenitors. To determine the transcriptional profile of embryonic phrenic neurons, and how they differ from other MNs, we isolated phrenic neurons from E11.5 *Hb9::GFP* mouse embryos. The genetic reporter labels axons and cell bodies of all spinal MNs (Wichterle et al., 2002). In cervical and thoracic trunk explants, the cell bodies of phrenic neurons were retrogradely labelled with the tracer TMR-dextran (Fig. 1A,B). Then, spinal cord segments C3-C5 were excised from the trunks, dissociated, and phrenic neurons were sorted as GFP^+ TMR^+ cells by flow cytometry (Fig. 1C). Immunohistochemistry confirmed that only $Pou3f1^+$ phrenic MNs in the medial-dorsal part of the ventral horn were TMR positive (Fig. 1B). As a control population, non-phrenic MNs were isolated from the same cell suspension. Given their segmental origin, these MNs are likely to represent a mix of MMC, HMC and LMC neurons (Peljto et al., 2010). A second control population of pure LMC neurons was isolated by retrograde labelling through the radial nerve (Fig. 1D,E). Following isolation by flow cytometry, genome-wide transcriptional patterns of phrenic neurons and the two control populations of MNs were determined using Affymetrix arrays.

Identification of phrenic neuron-specific genes

We next devised a scheme to systematically catalogue genes into groups based on their expression pattern in radial LMC MNs, phrenic MNs and non-phrenic control MNs derived from segments C3-C5, respectively. A logical value was attributed to each gene in

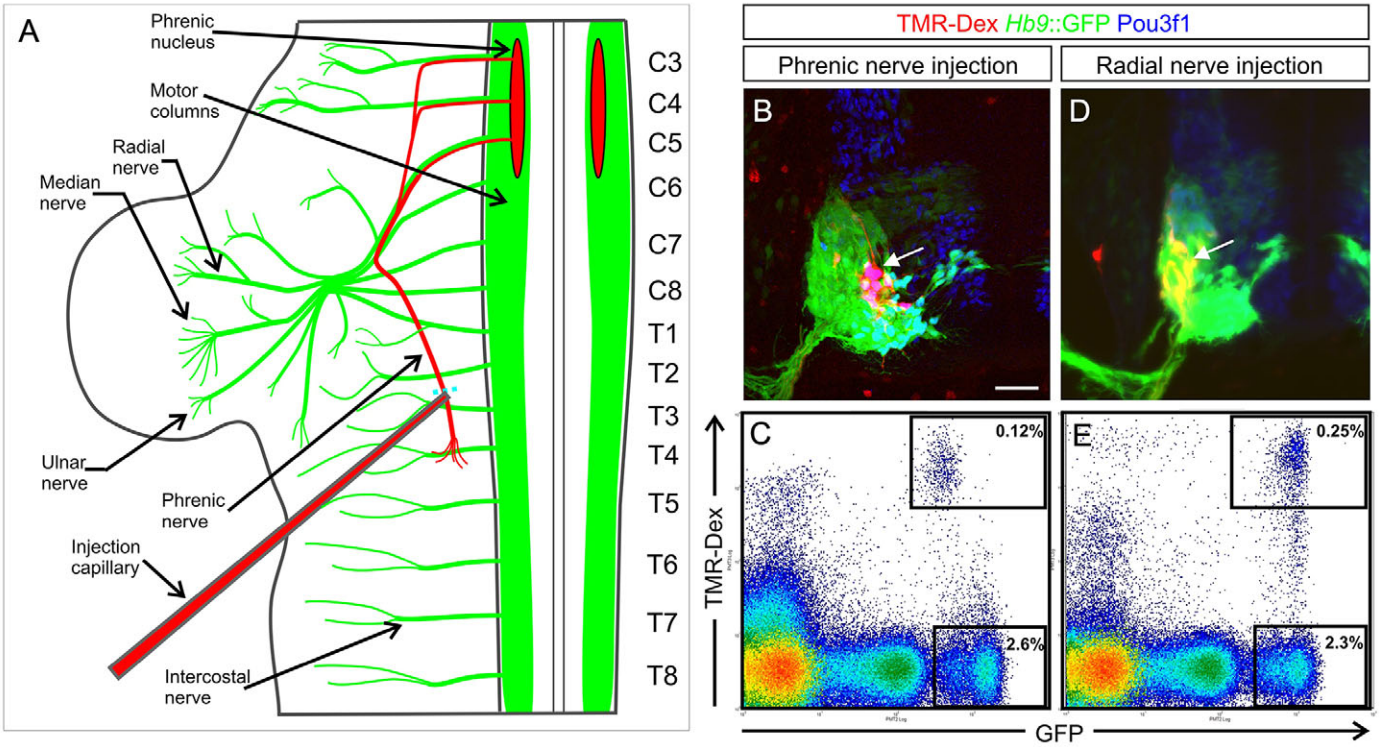

Fig. 1. Retrograde labelling and purification of mouse E11.5 embryonic phrenic MNs by flow cytometry. (A) The phrenic nerve was injected with TMR-dextran in *Hb9::GFP* trunk explants. Spinal segments are numbered according to the ventral roots that emerge from them (labels on right). C, cervical; T, thoracic. (B) Mid-cervical spinal cord transverse section: phrenic neurons (arrow) are labelled with TMR-dextran (red). The *Hb9::GFP* transgene labels all MNs; phrenic neurons co-express Pou3f1. Scale bar: 50 µm. (C) TMR^+ GFP^+ phrenic neurons and GFP^+ non-phrenic MNs were isolated from spinal cords (C3-C5 levels) by flow cytometry. (D) TMR^+ GFP^+ radial LMC neurons (arrow) in E11.5 cervical spinal cord (C6-C8 levels), following retrograde tracing through the radial nerve. (E) Purification of TMR^+ GFP^+ radial LMC neurons by flow cytometry.

Development (2014) doi:10.1242/dev.097188

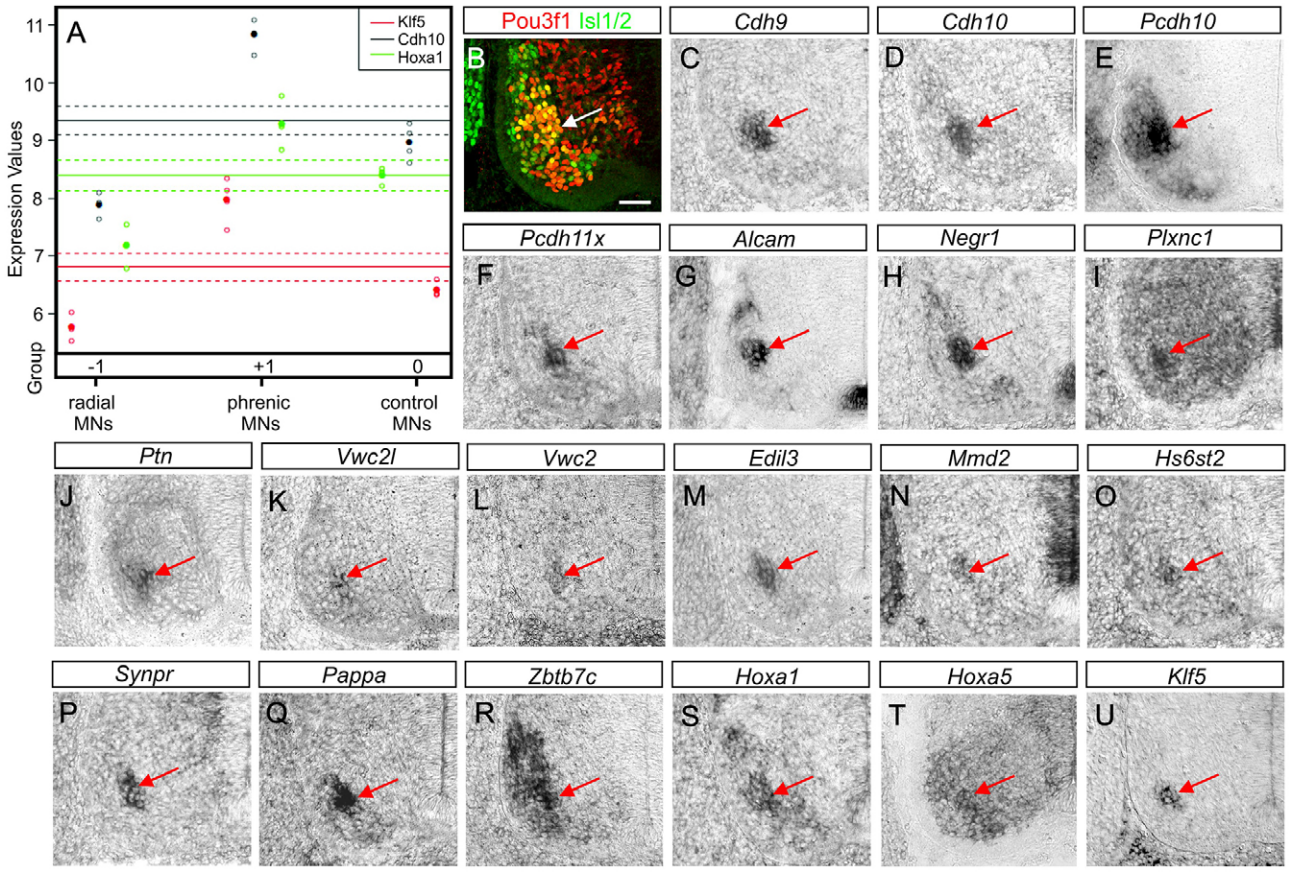

Fig. 2. Identification of genes enriched in phrenic neurons by Affymetrix array analysis. (A) Logical values were attributed to each gene in each cell type based on whether it is enriched (+1), within the mean (0) or depleted (−1). Three examples for genes enriched in phrenic neurons (*Klf5*, *Hoxa1*, *Cdh10*) are shown. Expression values are shown in $\log_2$ scale. (B) The PN is identified by expression of Pou3f1 and Isl1/2 in E11.5 mid-cervical spinal cords (arrow). Scale bar: 50 µm. (C-U) Candidate mRNAs are enriched in phrenic MNs. Red arrows indicate PN.

each cell population: genes expressed significantly above the mean across the three MN populations received the value +1, genes expressed significantly below the mean −1, and genes with expression levels above the 5th and below the 95th percentile around the mean received the value 0. *Hoxa1*, *Cdh10* and *Klf5* are examples of phrenic neuron-enriched genes with an expression value of −1 in radial MNs, +1 in phrenic MNs, and 0 in control MNs (Fig. 2A). This pattern can be described with the row vector [–1 +1 0].

A number of known MN subtype markers found in different groups of neurons suggest that our approach yields genuine expression patterns (Table 1). The MMC determinants *Lhx3* and *Lhx4* follow the pattern [–1 −1 +1] and are enriched in the C3-C5 control (Table 1), the only cell population with an MMC

Table 1. PN-enriched genes identified by Affymetrix array analysis

Enriched in PN	Examples for genes in group	Genes	Radial MNs	Phrenic MNs	Control MNs
No	*Dscam*	10	0	0	–1
No	*Gcnt2*	24	+1	0	–1
Yes	*Pappa*, *Alcam*	5	–1	+1	–1
Yes	***Tox***, *Pcdh10*, *Pcdh11x*	21	0	+1	–1
No	***Etv4***, ***Hoxc6***, *Cdh20*	78	0	–1	0
No	***Lhx1***, ***Hoxc8***, *Epha4*	63	+1	–1	0
No	***Hoxb6***, ***Hoxc5***	108	–1	0	0
No	***Etv6***, *Epha6*	277	+1	0	0
Yes	***Hoxa1***, ***Hoxa5***, *Cdh9*, *Cdh10*	173	–1	+1	0
Yes	***Arid5b***, ***Hey1***, ***Hey2***, *Plxnc1*	166	0	+1	0
No	***Lhx3***, ***Lhx4***	7	–1	–1	+1
No	***Runx2***	29	0	–1	+1
No	***Foxp1***, *Cdh7*	15	+1	–1	+1
No	***Hoxb5***, ***Nkx6-1***	52	–1	0	+1
No	***Rxrg***, ***Neurod1***	81	0	0	+1
No	***Hoxa4***, ***Pou3f1***, *Unc5c*	12	–1	+1	+1

PN-enriched genes are defined as (i) being significantly above the mean (+1) in phrenic neurons and (ii) within the 5th and 95th percentile around the mean or significantly below the mean (0 or −1, respectively) in the two control MN populations. Only selected genes are shown. Bold, TF; underlined, cadherin.

Development (2014) doi:10.1242/dev.097188

component. *Pou3f1*, one of the few established phrenic neuron markers (Bermingham et al., 1996; Rousso et al., 2008), is found both in phrenic neurons and C3-C5 control MNs. Subsequent expression analysis revealed that, at E11.5, *Pou3f1* is also expressed in a subset of MMC neurons (Fig. 2B; supplementary material Figs S3, S4), which explains the pattern that we observed. A second factor required for PN development, *Hoxa5* (Philippidou et al., 2012), is enriched in phrenic neurons as well. We were able to confirm phrenic neuron-specific expression for several candidate genes by *in situ* hybridisation (Fig. 2C-U). These genes fall into different functional categories and include cadherins (Fig. 2C-F), Ig superfamily receptors (Fig. 2G,H), BMP inhibitors (Fig. 2K,L), synaptic proteins (Fig. 2P) and TFs (Fig. 2R-U). The identification of phrenic MN-specific cadherins is significant, as adhesion molecules of this protein family are expressed in specific combinations on many, if not all, MN subsets. Cadherins mediate like-like clustering of MN cell bodies and drive the formation of topographic maps in the ventral spinal cord (Bello et al., 2012; Demireva et al., 2011; Price et al., 2002). In summary, we were able to identify a large number of genes potentially enriched in primary phrenic neurons and confirmed most of those analysed by histology.

An ESC-MN-based screening method for subtype determinants

To assess the efficacy of these genes to assign PN identity, we adapted the ESC-MN culture system such that we could perform GOF screens for multiple factors in purified MNs. We chose a mouse ESC clone that allows the efficient insertion of DOX-inducible transgenes by Cre/loxP-mediated cassette exchange (Iacovino et al., 2011) and equipped it with an additional MN-specific reporter transgene that allows magnetic enrichment of this cell type (Fig. 3A). During the initial phase of the project, we used ESCs carrying an *Hb9::CD2-GFP* MN-specific reporter (supplementary material Fig. S5, Table S2). To optimise the sorting procedure, we generated an ESC subclone that carries the *Hb9::CD14-IRES-GFP* transgene (supplementary material Fig. S1), which resulted in an improved signal-to-background ratio (Fig. 3B) and sorting efficiency. The GFP MN reporter tightly correlates with the endogenous embryonic MN marker Isl1/2 (Fig. 3C,D), and, following MACS, yielded large numbers (10^5-10^6) of viable, enriched ESC-MNs (Fig. 3B,E-G). Furthermore, we were able to induce the expression of candidate transgenes with DOX in culture, as shown here for the candidate factor Pou3f1 (Fig. 3H,I).

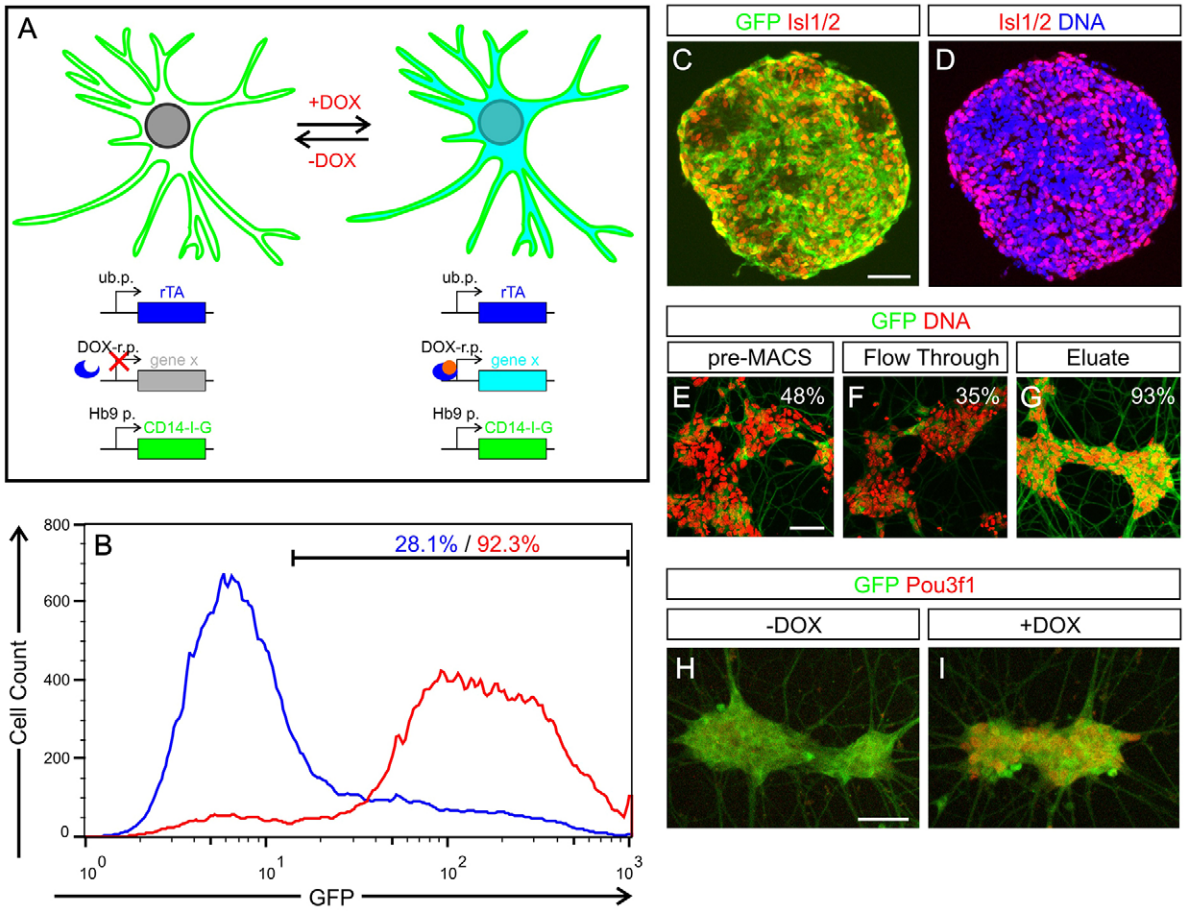

Fig. 3. Inducible expression of candidate phrenic determinants in sorted ESC-derived MNs. (A) GOF screen experimental setup for the identification of PN-specific transcriptional patterns. ESC-MNs were differentiated *in vitro*, isolated from mixed cultures with an MN-specific *Hb9::CD14-IRES-GFP* reporter gene and induced to express a given candidate gene with DOX. rTA, reverse Tet transactivator; ub.p., ubiquitous promoter; DOX-r.p., DOX-responsive promoter; Hb9 p., *Hb9* promoter. (B) Flow cytometry analysis of ESC-MNs enrichment by anti-CD14 MACS. Blue, pre-MACS cell suspension (dissociated EBs); red, anti-CD14-enriched MACS eluate. (C,D) GFP reporter and Isl1/2 expression in day 6 EBs differentiated from *Hb9::CD14-IRES-GFP* ESCs. (E-G) GFP-labelled MNs were enriched by anti-CD14 MACS and cultured (G), compared with the input (E) or the flowthrough (F). Percentage: GFP^+ cells. (H,I) DOX induction of iPou3f1 ESC-MNs cultured for 24 hours. Scale bars: 50 µm.

Development (2014) doi:10.1242/dev.097188

We next examined the subtype composition of parental ESC-MNs to determine the baseline identity in our assay. Primary mid-cervical MNs belong to three distinct subsets: HMC, MMC and PN (supplementary material Fig. S3A-G). When we compared the phenotypes of ESC-MNs with *in vivo* MNs, we found that they mostly belonged to the Pou3f1$^-$ Lhx3$^-$ HMC and the Pou3f1$^-$ Lhx3$^+$ or Pou3f1$^+$ Lhx3$^+$ MMC subsets, with only a small percentage of Pou3f1$^+$ Lhx3$^-$ phrenic-like neurons (supplementary material Fig. S3H-L), consistent with an earlier study (Peljto et al., 2010). The percentage of ESC-MNs with an MMC phenotype declines between day 5 and day 6 (supplementary material Fig. S3L). This might be explained by the fact that all MN progenitors express Lhx3 initially, but only MNs committed to the MMC fate sustain its expression (Sharma et al., 1998). The MN subtype composition does not depend on the ESC clone used in this study, as we have detected similar ratios of MN subtypes in cultures differentiated from a second, independently derived ESC clone (supplementary material Fig. S3M).

Our analysis of genes enriched in primary phrenic neurons pinpointed a cluster of known and putative TFs that would be good candidates as determinants of PN identity (Table 1; supplementary material Table S1). In cases in which two closely related genes were isolated, only one gene was investigated further. Our transcriptional profile also identified Notch signalling as a potential key player in this process, as we found that Notch targets, such as *Hey1* and *Hey2* (Table 1), are enriched in phrenic neurons. Furthermore, we included a dominant-negative mutant form of Lhx3 (DNLhx3) (West et al., 2004) because DNLhx3 suppresses Lhx3 target genes and might inhibit this key MMC determinant (Agalliu et al., 2009). *Vwc2* was the only non-TF chosen for analysis, because it is a chordin-like BMP inhibitor and may modulate neural patterning. Finally, we selected *Hoxc6* and wild-type *Lhx3* as control TFs, as they represent known LMC and MMC determinants, respectively. We established 19 sets of ESC subclones carrying single candidate transgenes (supplementary material Table S2) and confirmed inducible candidate gene expression in embryoid bodies (EBs) (supplementary material Fig. S6).

Reconstruction of PN-specific transcriptional patterns in ESC-MNs

To address whether candidate determinants promote transcriptional profiles associated with phrenic neurons when ectopically expressed in ESC-MNs, we differentiated transgenic ESCs into MNs in EB cultures. MNs were magnetically sorted from dissociated EBs on day 5 and induced to express the transgene with DOX during the subsequent 30 hour culture period. In some experiments with Notch constructs, the ESC-MNs were only induced for the last 10 hours to limit the effect of the transgenes. RNA of ESC-MNs derived from two independent subclones for each candidate gene was isolated, and gene expression profiles determined using Affymetrix arrays. The expression data are represented as a scatter plot in Fig. 4, in which the number of PN-enriched genes (supplementary material Table S4) repressed/induced (*y*-axis) is plotted against all genes repressed/induced by a given candidate factor (*x*-axis). The mean value for each transgene is represented by two data points, one for repression (lower left quadrant) and one for induction (upper right quadrant). We would like to point out that the terms repression and induction do not necessarily imply a direct genetic interaction, as we measure mRNA levels and not promoter binding.

Thus, the lower the *y*/*x* ratio for repression (*R*-ratio) and the higher the *y*/*x* ratio for induction (*I*-ratio) the more the transcriptional pattern evoked by a transgene approximates that of primary phrenic neurons. The *P*-values obtained using a hypergeometric distribution for over-representation of induced or repressed genes (supplementary material Table S5) provide a very similar picture to that offered by the *R*- and *I*-ratios, except that these results are more difficult to visualise.

Of all candidate determinants tested, ESC-MNs overexpressing Pou3f1 showed the most specific induction of PN-enriched genes (*I*-

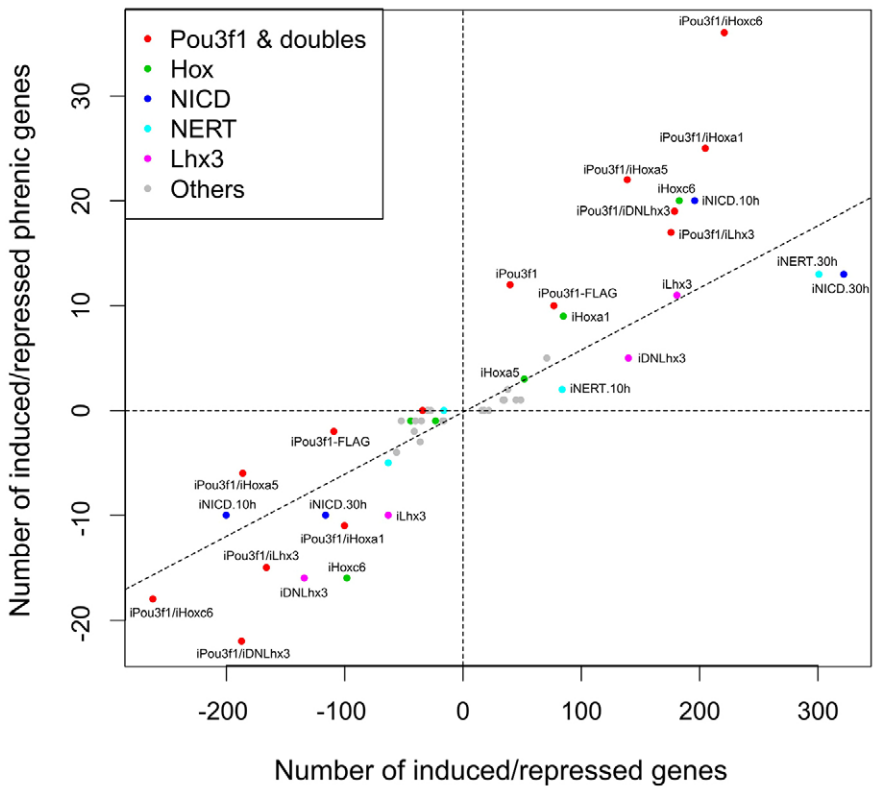

Fig. 4. Identification of TFs that control parts of the PN-specific transcriptional pattern. MACS-sorted ESC-MNs were induced to express candidate determinants, and their transcriptional profiles were examined by Affymetrix array analysis. In the scatter plot, the number of PN-specific genes induced/repressed (*y*-axis) is plotted against the number of all genes induced/repressed (*x*-axis) by a given candidate factor or combination thereof. The diagonal line represents a robust fit through all the points shown, both induced and repressed.

Development (2014) doi:10.1242/dev.097188

ratio=0.3; Fig. 4, upper right quadrant), whereas not a single specific gene is repressed (*R*-ratio=0). The genes upregulated by Pou3f1 include the confirmed PN-specific genes *Cdh9*, *Cdh10* and *Pcdh11x* (Fig. 2C,D,F). NICD, when DOX-induced for the last 10 hours of ESC-MN culture, was identified as a second PN-candidate factor with a high *I*-ratio (0.102) and low *R*-ratio (0.05) (Fig. 4; supplementary material Fig. S7A). The set of PN-specific genes upregulated by iNICD includes *Vwc2l* (Fig. 2K) and is largely non-overlapping with that observed in inducible (i) Pou3f1 ESC-MNs (supplementary material Fig. S8A, Table S6), although a few target genes, such as *Hs6st2*, are shared. The timing and signal intensity of Notch activity appear to be critical, as iNICD expressed for 30 hours, or the attenuated mutant isoform iNERT (Schroeder et al., 2003) induced for 10 hours or 30 hours, do not evoke a PN-like pattern. iHoxc6, despite the absence of *Hoxc6* from primary phrenic neurons (Table 1), has a high *I*-ratio (0.109), yet also a high *R*-ratio (0.163) (supplementary material Fig. S7B). However, although iHoxc6 does induce 20 PN-enriched genes, including *Hoxa5* (supplementary material Table S6), it also upregulates two key LMC determinants, *Foxp1* (Dasen et al., 2008) and *Aldh1a2* (Sockanathan and Jessell, 1998) (supplementary material Table S7). Ectopic iHoxa5 expression in ESC-MNs, by contrast, does not induce these LMC markers, and positively regulates only three phrenic neuron-enriched genes, including *Ptn* (Fig. 2J; supplementary material Table S6). Thus, when activated in isolation, iHoxa5 does not emulate a PN transcriptional programme. Finally, iDNLhx3 does not evoke PN-like patterns (Fig. 4), but surprisingly shows the best *I*-ratio for LMC-like patterns (supplementary material Fig. S9, Tables S5, S7). This suggests that repression of Lhx3 targets unlocks parts of the LMC but not of the PN transcriptional programme in ESC-MNs.

Pou3f1 interacts with Hoxa5 to establish a phrenic-like transcriptional profile *in vitro*

To explore whether any of the candidate determinants interact to elicit PN-like transcriptional patterns, we combined the most promising candidate, Pou3f1, with Hoxa5, Hoxc6, Hoxa1 and DNLhx3 in an expression system that allows us to simultaneously induce two candidate genes in the same ESC-MNs (Bondue et al., 2011). In addition, we combined Pou3f1 with Lhx3 to investigate negative interactions, as we observed that Pou3f1 target genes, such as *Cdh9* and *Cdh10* (Fig. 2C,D), are restricted to the PN, whereas Pou3f1 itself is also expressed by a subpopulation of the MMC (supplementary material Figs S3, S4) (Rousso et al., 2008). Array analysis of double-transgenic ESC-MNs revealed that iPou3f1/iHoxa5 and iPou3f1/iHoxc6 DOX induction resulted in nearly identical *I*-ratios (0.158 versus 0.163; Fig. 4; supplementary material Fig. S7C). By contrast, the *R*-ratio for iPou3f1/iHoxa5 (0.032) indicates higher specificity than that for iPou3f1/iHoxc6 (0.069). As in the iHoxc6 single-transgenic ESC-MNs, iPou3f1/iHoxc6 expression upregulates the LMC determinants *Foxp1* and *Aldh1a2*, whereas iPou3f1/iHoxa5 expression does not (supplementary material Table S7). Interestingly, the number of PN-specific genes activated above the twofold threshold in iPou3f1/iHoxa5 ESC-MNs (22 genes) is higher than the sum of the two target gene sets in single transgenic MNs (12+3 genes), which suggests that several PN target genes, such as *Pcdh10*, require the combined activity of both determinants (supplementary material Table S6). Comparison of transcriptional patterns of iPou3f1 and iPou3f1/iLhx3 ESC-MNs shows that four of 12 iPou3f1-induced PN-specific targets, including *Cdh9*, are downregulated more than twofold by co-expression of Lhx3 (supplementary material Fig. S7D, Table S6). These findings provide evidence that Pou3f1 can interact with other determinants to regulate the activation of PN-specific target genes, and that both positive (Hoxa5) and negative (Lhx3) combinatorial interactions can be observed in ESC-MNs. Furthermore, Hoxa5 and Hoxc6, despite considerable overlap in their target genes (supplementary material Fig. S8B), differ in that Hoxc6 initiates LMC-like transcriptional patterns in ESC-MNs, whereas Hoxa5 does not.

In order to validate the transcriptional patterns observed by array analysis, we tested the expression of selected candidate genes in iYFP, iHoxa5, iNICD (10 hour pulse), iPou3f1 and iPou3f1/iHoxa5 ESC-MNs by qRT-PCR (supplementary material Table S8). The qRT-PCR expression data are largely consistent with the array data, although some additional target genes were detected. Crucially, the qRT-PCR analysis showed that NICD upregulates the PN determinant *Pou3f1*.

Notch signalling induces the PN determinant Pou3f1 in MNs *in vitro* and *in vivo*

Do the three positive phrenic determinants we identified simply act in parallel or is there a transcriptional hierarchy, i.e. does one of the candidate factors initiate phrenic neuron specification? As the qRT-PCR data suggested that NICD activity upregulates *Pou3f1*, we further examined a possible hierarchical relationship between the two factors. We compared EBs derived from the parental ESC line with those derived from iNERT ESCs, which express an attenuated, tamoxifen (4HT)-inducible version of NICD (Fig. 5A-F). Even in the absence of induction with DOX and 4HT, iNERT EBs contained a significantly higher proportion of both phrenic-like Pou3f1$^+$ Lhx3$^-$ MNs and MMC-like Pou3f1$^+$ Lhx3$^+$ MNs (Fig. 5G), without a change in total MN numbers. This increase is likely to be caused by low-level transgene expression/activity in the absence of added inducers, which is a common phenomenon seen in inducible genetic systems (Howe et al., 1995; Schroeder et al., 2003). Full induction of the iNERT transgene led to a decrease in the number of MNs (Fig. 5E,F), consistent with previous findings when NICD was overexpressed in spinal progenitors *in vivo* (Dias et al., 2012). We next examined whether Notch signalling is required for Pou3f1 expression in a subset of normal ESC-MNs. We treated developing EBs with γ-secretase inhibitors, which block ligand-dependent Notch activation (De Strooper et al., 1999). Both of the inhibitors that we tested decreased the percentage of Pou3f1$^+$ ESC-MNs by more than 90% (Fig. 5H-N), whereas they did not affect MN development in general. To test if Notch GOF upregulates additional PN markers, we examined the effect of a 10 hour pulse of DOX on the transcriptional patterns of iNICD EBs and cultured ESC-MNs, compared with normal controls. We found that NICD induces the PN-enriched genes *Synpr* (supplementary material Fig. S10), *Cdh9*, *Cdh10*, *Pcdh11x* and *Ptn* (supplementary material Table S8).

Given that Notch activity controls Pou3f1 in MNs *in vitro*, does the presence of a Notch ligand correlate with the appearance of Pou3f1$^+$ MNs *in vivo*? Analysis of mid-cervical ventral spinal cord revealed that at E10.5, which is when MNs emerge from the pMN domain, a cluster of *Dll4*-positive cells is located just dorsal of nascent Pou3f1$^+$ Isl1/2$^+$ MNs (Fig. 6A,B). Previous studies have mapped *Dll4* expression to the p2 progenitor domain (Del Barrio et al., 2007; Peng et al., 2007). Furthermore, Notch1 protein is detectable on the most immature, medial MNs, and Pou3f1 expression in MNs overlaps with that of the Notch target gene *Hey1* (supplementary material Fig. S11). At E11.5, Pou3f1$^+$ MNs have migrated laterally to settle in the PN and the MMC (Fig. 6D), a pattern that remains unchanged at E12.5 (Fig. 6G). *Dll4* expression, by contrast, is transient and not seen at later time points (Fig. 6E,H),

Development (2014) doi:10.1242/dev.097188

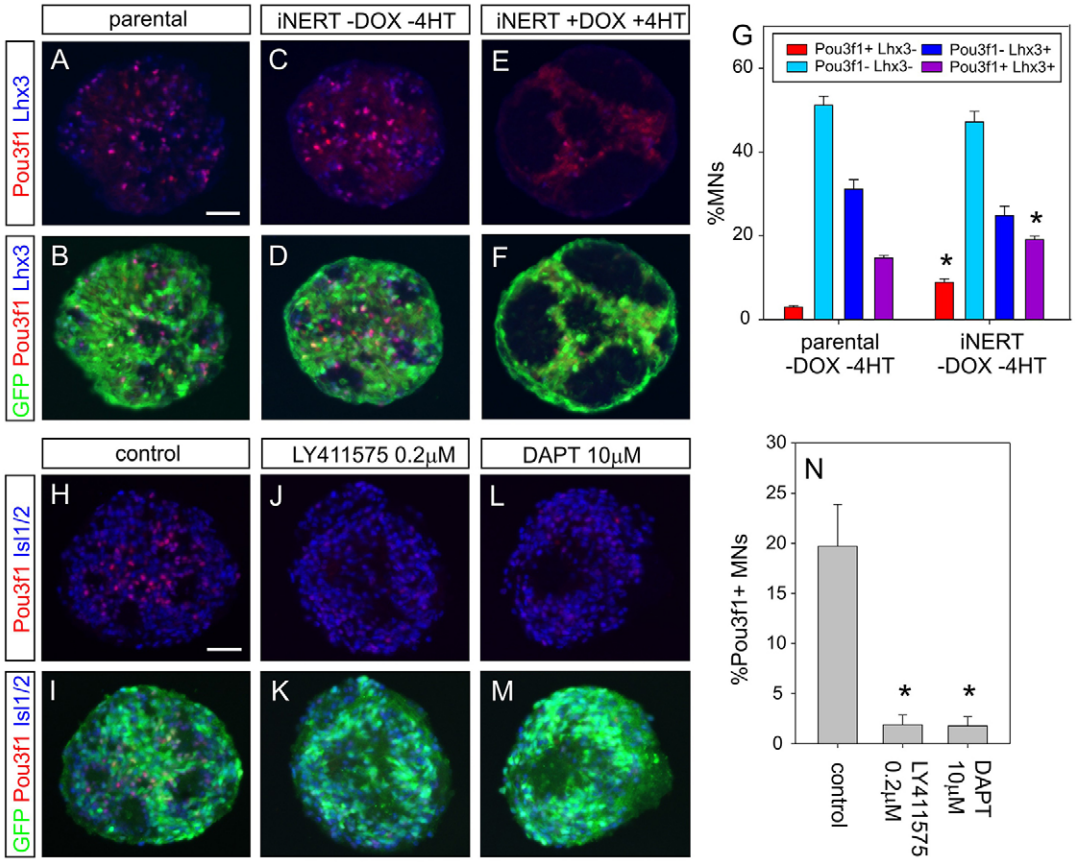

Fig. 5. Notch activation regulates Pou3f1 expression in ESC-derived MNs. (A-F) GFP, Lhx3 and Pou3f1 staining in day 6 EBs derived from parental H14IG#E3 ESCs and iNERT ESCs (without and with DOX/4HT induction). (G) Percentages of Pou3f1$^+$ Lhx3$^-$ (PN-like, red), Pou3f1$^-$ Lhx3$^-$ (HMC-like, light blue), Pou3f1$^-$ Lhx3$^+$ (dark blue) and Pou3f1$^+$ Lhx3$^+$ (purple) cells among ESC-derived GFP$^+$ MNs in day 6 EBs. The EBs were derived from ESC clones H14IG#E3 and iNERT without DOX/4HT induction. (H-M) GFP, Pou3f1 and Isl1/2 labelling in day 6 EBs. EBs were either differentiated according to the standard protocol (H,I) or treated the γ-secretase inhibitors LY411575 (J,K) or DAPT (L,M) from day 2 onwards. (N) Percentages of Pou3f1$^+$ MNs among all GFP$^+$ MNs in the absence or presence of γ-secretase inhibitor. Error bars indicate mean values from three independent experiments ± s.e.m. (G,N). *P<0.05 (paired Student's t-test). Scale bars: 50 μm.

except in blood vessels. The expression of the Pou3f1 target gene *Cdh10* is delayed compared with Pou3f1 itself and is first detected in the PN at E11.5 (Fig. 6C,F,I). The juxtaposition of Pou3f1 and *Dll4 in vivo* is mirrored by the pattern that we see in EBs, where patches of Pou3f1$^+$ Isl1/2$^+$ MNs are localised close to *Dll4*$^+$ non-MNs (Fig. 6J,K).

To examine whether Dll4 protein is capable of inducing Pou3f1 expression in primary MNs, we used whole embryo culture (WEC) (Osumi and Inoue, 2001) to ectopically express this Notch ligand in cervical spinal cords of intact mouse embryos. Owing to the timing of the WEC cultures, many non-MNs in close proximity to Isl1/2$^+$ MNs and ventral progenitors express the co-transfected reporter nGFP (Fig. 6L,N), whereas MNs themselves are mostly negative. Hence, any effect seen in MNs is likely to be non-cell-autonomous. Embryos developed normally in culture and formed a Pou3f1$^+$ PN (Fig. 6L-O). In DLL4-transfected embryos (Fig. 6L,M), but not in controls (Fig. 6N,O), the transfected side of the spinal cord contains significantly more MNs of phrenic phenotype (Fig. 6P). At the same time, the total number of MNs is unchanged (Fig. 6P), suggesting that ectopic expression of DLL4 does not expand MN progenitors. Taken together, these findings show that Pou3f1 induction in embryonic MNs is controlled by Notch signalling both in ESC-MNs and *in vivo*, and suggest that Delta-Notch interaction is involved in the acquisition of phrenic neuron identity.

The PN-specific receptors Cdh10 and Pcdh10 mediate cell clustering of ESC-MNs

A key event in early MN patterning is the aggregation of MNs of the same subtype into clusters/nuclei within the ventral horn. This like-like recognition of cell bodies is mediated by receptors of the cadherin family. Expression profiling of primary MNs suggested that the cadherins Cdh10 and Pcdh10 are highly enriched in the PN (Fig. 2D,E). To examine whether these potential effector genes are sufficient to drive specific MN clustering, we ectopically expressed Cdh10 or Pcdh10 in ESC-MNs and mixed them with RFP-labelled control ESC-MNs (Fig. 7A-C). Near-neighbour analysis revealed that iCdh10 MNs and iPcdh10 MNs, but not RFP$^-$ control MNs, segregated from RFP$^+$ control MNs in culture and formed nucleus-like aggregates (Fig. 7D-J).

DISCUSSION

The development of phrenic neurons, which drive respiration in mammals, requires the integration of positional signals to restrict their specification to mid-cervical segments of the spinal cord, where they emerge in register with myoblasts destined to form their target muscle, the diaphragm (Babiuk et al., 2003). We performed expression profiling in primary embryonic neurons followed by the reconstruction of phrenic-like transcriptional patterns in transgenic ESC-MNs to identify factors that combine

Development (2014) doi:10.1242/dev.097188

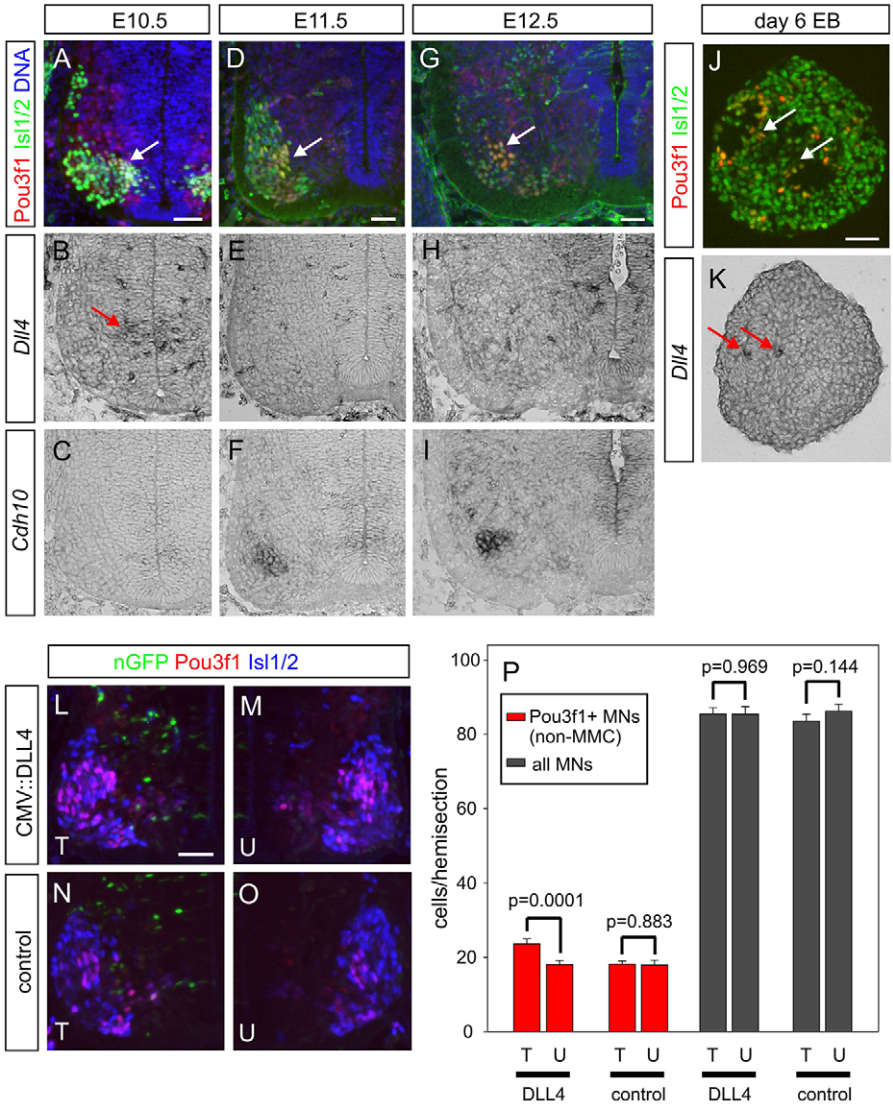

Fig. 6. The Notch ligand *Dll4* is expressed adjacent to nascent Pou3f1$^+$ MNs and induces Pou3f1 in primary embryonic MNs. (A,D,G) Expression of Pou3f1 and the pan-MN marker Isl1/2 in E10.5, E11.5 and E12.5 mid-cervical spinal cord. Phrenic neurons are labelled by both markers (arrow). (B,E,H) Red arrow indicates *Dll4* expression at E10.5. At E11.5 and E12.5, few *Dll4*$^+$ cells are visible, apart from blood vessels. (C,F,I) *Cdh10*, a Pou3f1 target gene, labels phrenic neurons at E11.5 and E12.5. (J) Day 6 EBs stained for Isl1/2 and Pou3f1; arrows indicate double-positive cells. (K) Expression of *Dll4* in small patches of day 6 EBs (arrows). The sections in J and K are adjacent. (L-O) Mid-cervical spinal cords of mouse embryos transfected with expression vectors for human DLL4 and nGFP (L,M) or mock and nGFP (N,O) at ~E9.75 and then allowed to develop in WEC for 40 hours. Sections were stained for nGFP, Isl1/2 and Pou3f1. (P) Analysis of mean numbers of Pou3f1$^+$ Isl1/2$^+$ MNs outside the MMC (red bars) and all Isl1/2$^+$ MNs (black bars) in mid-cervical spinal cord hemi-sections of transfected embryos. Error bars indicate mean values from four (DLL4) or three (control) embryos ± s.e.m. (25 pairs of images each). *P*-values are by paired Student's *t*-test. Similar significances were obtained using the Mann-Whitney test and logistic regression. T, transfected side; U, untransfected side. Scale bars: 50 µm.

to establish PN identity along the dorsoventral and anteroposterior axes of the spinal cord. We found that three factors, Pou3f1, Hoxa5 and Notch, interact to control sets of putative PN-specific effector genes: Hoxa5 only evokes PN-like transcriptional patterns when combined with Pou3f1, and Notch signalling is upstream of Pou3f1. The latter interaction was observed both in ESC-MNs and in spinal cords of intact mouse embryos. Thus, our study suggests that Delta-Notch signalling at the dorsal margin of the nascent motor columns has to intersect with Hox5-dependent mid-cervical segmental identity for phrenic neurons to develop (Fig. 8). Given that NICD controls *Pou3f1*, why is there only a limited overlap between their target genes in ESC-MNs (supplementary material Fig. S8A)? The most likely explanation for this is the short time frame of iNICD induction (10 hours), which is sufficient to upregulate *Pou3f1* itself (supplementary material Table S8) but not second-order Pou3f1 targets. Based on co-expression assays in ESC-MNs, we also predict that Lhx3 is a negative regulator of phrenic identity in Pou3f1$^+$ MMC neurons. In addition to transcriptional determinants, we identified and validated several sets of putative PN effector genes downstream of these regulators of PN identity. Many of these genes are regulated in a modular fashion by single factors, whereas others require the combined activity of two determinants.

The aggregation of MNs that connect to the same target muscle into nuclei and motor pools is a key event in early MN development and depends on MN subtype-specific expression of cadherins (Bello et al., 2012; Demireva et al., 2011; Price et al., 2002). This establishes a topographic map of MN cell bodies within the ventral horn and ensures that functionally related MNs receive the same sensory synaptic input (Sürmeli et al., 2011), as well as facilitating the formation of electrical synapses between MNs to coordinate activity (Personius et al., 2007). We found that the phrenic neuron-enriched receptors Cdh10, which is regulated by Pou3f1, and Pcdh10 (Hirano et al., 1999), which is regulated by Hoxa5 and Pou3f1, mediate like-like clustering of ESC-MN cell bodies *in vitro* (Fig. 7, Fig. 8C) and may contribute to the aggregation of phrenic neurons into the PN, probably in concert with other adhesion molecules.

Our findings on PN specification in ESC-MNs suggest that the coordinated expression of cadherins and other effector genes in phrenic neurons depends on the combinatorial activity of at least three positive and one negative determinant. Nevertheless, our understanding of PN gene regulation remains incomplete. For example, we do not know how the PN-enriched receptor genes *Alcam* and *Plxnc1* are regulated. There are a number of possible explanations for the limitations to our approach: (1) additional,

Development (2014) doi:10.1242/dev.097188

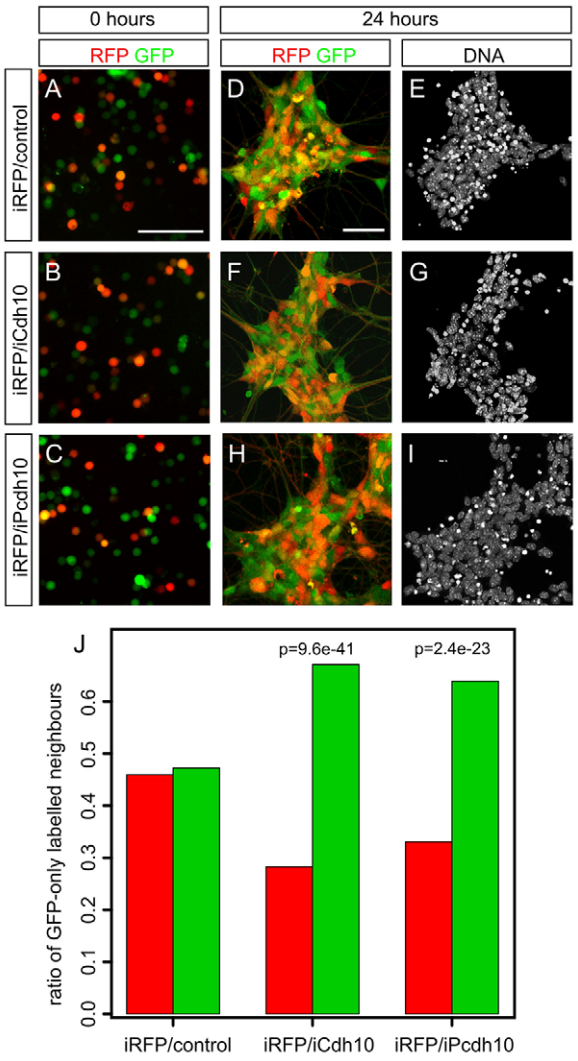

Fig. 7. The PN-specific cadherins Cdh10 and Pcdh10 mediate specific clustering of ESC-MNs. (A-C) GFP-only and RFP$^+$ GFP$^+$ ESC-MNs are randomly mixed at 0 hours. (D-I) Mixed cultures of GFP-only and RFP$^+$ GFP$^+$ ESC-MNs aggregate within 24 hours. (J) Analysis of like-like clustering of ESC-MNs in mixed cultures (24 hours) by near-neighbour analysis. Bar colours indicate the label of the central cell: red, RFP$^+$ GFP$^+$ control MNs; green, GFP-only control, iCdh10 or iPcdh10 MNs. *P*-values were calculated based on the generalised linear model with random effects. The chart shows pooled data from three independent experiments. Eight to ten cell clusters per condition (2267 MNs total) were scored. Scale bars: 50 µm.

unknown transcriptional determinants might positively regulate additional sets of PN-selective genes; (2) ESC-MNs might contain more negative regulators, which mask aspects of induced PN identity; (3) peripheral cues encountered by outgrowing phrenic axons might control some PN target genes, and these cues would not be present *in vitro*; (4) some of the PN-enriched genes that are not yet confirmed by histology could be false positives, in particular those in the least stringent [0 +1 0] group (supplementary material Table S4).

The two cervical Hox genes *Hoxa5* and *Hoxc6* evoked strikingly similar transcriptional patterns when overexpressed in ESC-MNs as single transgenes (supplementary material Fig. S8B) or combined with Pou3f1 (supplementary material Table S7), consistent with the fact that different cervical Hox proteins can bind to the same consensus DNA site (Pellerin et al., 1994). Co-expression of iPou3f1 plus iHoxa5 revealed combinatorial effects, and the overall PN specificity of the pattern is higher than that of iPou3f1 plus iHoxc6. Crucially, iHoxc6 and iPou3f1 plus iHoxc6, but not iHoxa5 and iPou3f1 plus iHoxa5, induce the TF *Foxp1*. This key LMC determinant, which largely depends on Hox6 expression *in vivo* (Dasen et al., 2008; Lacombe et al., 2013), suppresses PN identity when ectopically expressed in cervical MNs (Rousso et al., 2008). Thus, the combination of iPou3f1 plus iHoxc6 induces an LMC-type programme that is similar to that of the PN, yet at the same time is incompatible with PN identity. An *in vivo* correlate to the *Foxp1*-positive iPou3f1/iHoxc6 ESC-MNs indeed exists: ulnar motor pools, which are caudal LMC subpopulations that innervate distal limb muscles in mice (Lacombe et al., 2013), and anatomically related flexor carpi ulnaris MNs in chick (Dasen et al., 2005) co-express Pou3f1 and Hoxc6 during its initial specification. Despite their different identities, aspects of the subtype-specific genetic programmes are shared between the PN and ulnar MNs, as both populations selectively express the Pou3f1 target genes *Cdh9* and *Cdh10* (Fig. 2B-D; supplementary material Fig. S12).

MN subtype identity has been linked to Notch signalling: in *Gde2* (*Gdpd5*) null mutant mice, which have increased levels of activated Notch, MNs show a marked shift in columnar subtype composition (Sabharwal et al., 2011). Intriguingly, in their study, Notch affects MN fate at the level of progenitor cells. We first observe Pou3f1 upregulation in Isl1/2$^+$ postmitotic MNs (Fig. 6A). Nevertheless, we do not know whether Notch induction of this key PN determinant occurs before or after cell cycle exit. Delta-Notch interaction as a mechanism to diversify V2a/V2b spinal interneurons appears to be conserved between fish, birds and mammals (Batista et al., 2008; Del Barrio et al., 2007; Peng et al., 2007). There are two scenarios of how the ancestral Dll4$^+$ territory in the p2 progenitor domain, which drives this process, might relate to the emergence of the PN during mammalian evolution. In the first scenario, Dll4 expression might have acquired a novel role in establishing the mammal-specific PN. This would imply that phrenic neurons arose from cervical HMC neurons, which were respecified by Delta-Notch signalling, as the diaphragm evolved from cervical hypaxial muscle (Perry et al., 2010). Alternatively, the PN might be an evolutionary modification of an ancestral LMC subset that predates mammals. Hirasawa and Kuratani recently proposed that the diaphragm originated from limb muscle associated with the pectoral girdle (Hirasawa and Kuratani, 2013). If this scenario is correct, then phrenic neurons might have evolved from a Pou3f1$^+$ LMC subset that lost its brachial Hox code due to a duplication of two cervical segments coupled with a caudal shift in brachial identity, an event that might have occurred during early mammalian phylogeny (Hirasawa and Kuratani, 2013). This view is supported by the fact that, in mammals, there are two Pou3f1$^+$ MN subsets spaced by about two segments at cervical levels, one rostral of the LMC (the PN) and one caudal within the LMC (ulnar MNs).

In this study, we have demonstrated that MN derivation from ESCs is a viable screening tool to systematically dissect developmental pathways. Our experimental strategy was based on initially identifying candidate determinants in sorted primary embryonic neurons by transcriptional profiling and then validating the factors in the ESC-derived equivalent of these *ex vivo* cells. Both a highly reductionist approach (genome-wide expression analysis in ESC-MNs) and the more complex, heterogeneous EB culture system provided insights into how a network of TFs interact to establish PN identity. Similar ESC-based screens could be undertaken for other cell types that are difficult to access in large numbers. We think that the derivation of MNs from pluripotent stem cells will mature into

Development (2014) doi:10.1242/dev.097188

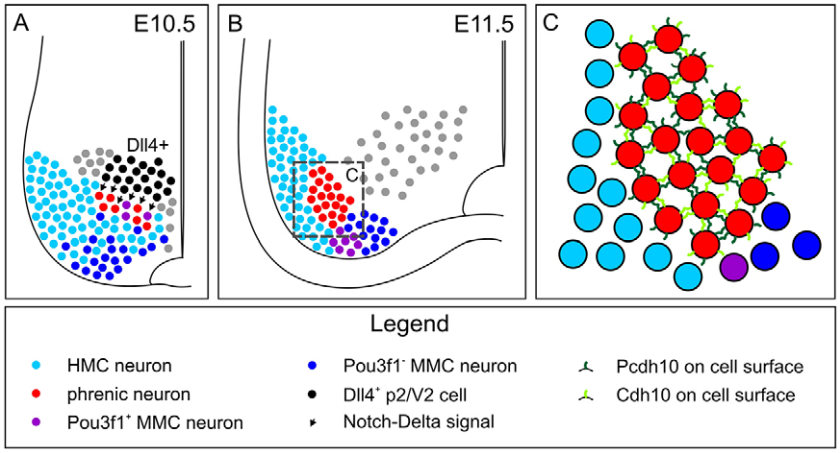

Fig. 8. Model of Delta/Notch induction of phrenic neuron identity. (A) At E10.5, Dll4-positive p2 progenitors and V2 interneurons are located immediately dorsal of nascent MNs. MNs committed to MMC or HMC fate adjacent to Dll4$^+$ territory fate are exposed to Notch signalling and upregulate the phrenic neuron determinant Pou3f1. Other Notch ligands expressed in the embryonic spinal cord might also contribute to this process. (B) Following their specification by Delta/Notch, Pou3f1$^+$ phrenic neurons migrate laterally and settle into a medial position next to the HMC. (C) The Pou3f1 targets Cdh10 and Pcdh10 mediate like-like clustering of phrenic MNs and contribute to the formation of the PN.

a powerful tool to investigate not only prenatal developmental programmes, but also subtype-dependent features of adult MN function and connectivity, complementing existing animal models. Our long-term aim is to assemble adult-like phrenic ESC-MNs, as well as other defined cell types, into artificial neuromuscular circuits to simulate aspects of respiratory motor function in health and disease *in vitro*. The progress towards understanding embryonic phrenic neuron identity reported here will allow us to extend the investigation to later steps of neuronal maturation and circuit formation.

MATERIALS AND METHODS

Summary

Embryonic phrenic neurons were labelled by injecting a retrograde tracer (TMR-dextran) into the phrenic nerve in E11.5 trunk explants derived from mouse embryos carrying the *Hb9::GFP* transgene (Wichterle et al., 2002). Explants were cultured in an oxygenated bath for 2 hours and then dissociated with papain, and TMR$^+$ GFP$^+$ phrenic neurons, as well as GFP$^+$ control MNs, isolated by flow cytometry (Fig. 1A-C). In separate experiments, radial LMC neurons were retrogradely labelled and isolated using the same methodology. Gene expression profiles of sorted primary MNs were determined by Affymetrix array analysis.

MNs were directly differentiated *in vitro* from mouse ESCs as described (Peljto et al., 2010). Briefly, A2.lox ESCs (Iacovino et al., 2011) carrying the MN-specific, magnetically sortable reporter genes *Hb9::CD2GFP* or *Hb9::CD14-IRES-GFP* (supplementary material Fig. S1) were grown for 2 days as EBs, induced with 1 µM retinoic acid and 0.5 µM smoothened agonist (SAG), and dissociated on day 5. MNs were then isolated by magnetically activated cell sorting (MACS). MACS-purified ESC-MNs were cultured for 30 hours on Matrigel, and the expression of PN-specific candidate genes (supplementary material Tables S1, S2) was induced with doxycycline (DOX). Then, transcriptional profiles of ESC-MNs were determined by Affymetrix array analysis and qRT-PCR (Spandidos et al., 2010) (supplementary material Table S3). ESC-MNs expressing the neutral transgene YFP were used as the baseline, as the DOX-inducible Cre recombinase present in the parental ESC line triggers a DNA damage response in MNs (supplementary material Fig. S2).

Detailed protocols are available in supplementary Materials and Methods.

Acknowledgements

We thank Tom Jessell and Andrew Lumsden for support and encouragement; Noriko Osumi and Yoko Arai for advice on WECs; Ira Schieren, Kaity Miao and Fazal Oozeer for expert technical assistance; Jeremy Dasen, Fiona Watt, Robert Knight, Linda Greensmith, Christopher E. Henderson, QueeLim Ch'ng, Stephen Price and Anthony Graham for comments on the manuscript; Chris G. Tan for sharing unpublished observations; and Austin Smith, Esteban O. Mazzoni, Hynek Wichterle, Koichi Kawakami, Cedric Blainpain, Dafe A. Uwanogho, Shinji Hirano, Ursula Just, Malcolm Logan, Linda Greensmith, Matthew Grist, Uwe Drescher and Simon J. Rhodes for providing reagents.

Competing interests

The authors declare no competing financial interests.

Author contributions

C.B.M., I.L., M.N., K.C.K. and P.K. generated DNA constructs. C.B.M., I.L., P.K., D.S., M.C. and M.N. established and characterised ESC subclones. C.B.M. and I.L. derived MNs from ESCs, MACS sorted them and analysed them by flow cytometry and microscopy. M.I. and M.K. contributed the A2lox.Cre ESC clone prior to its publication. I.L. isolated primary MN populations from embryos and D.C. determined their transcriptional patterns. K.C.K. contributed to the original concept of the study. E.B. developed the strategy for large-scale comparison of transcriptional patterns and performed statistical analysis. C.B.M., E.B. and I.L. wrote the manuscript and assembled the figures. I.L. developed the original concept, designed and oversaw the study.

Funding

Personnel and work were supported by the Medical Research Council [grant G0900585, I.L.]. Additional funding was provided by the Thierry Latran Foundation (I.L.); the Biotechnology and Biological Sciences Research Council [grant G1001234, I.L. and Britta Eickholt, KCL/Charité, Berlin, Germany]; Project ALS (K.C.K.) and the Tow Foundation (K.C.K.). K.C.K. was the recipient of a Kirschstein-NRSA Fellowship from NINDS, National Institutes of Health. Deposited in PMC for immediate release.

Supplementary material

Supplementary material available online at
http://dev.biologists.org/lookup/suppl/doi:10.1242/dev.097188/-/DC1

References

Agalliu, D., Takada, S., Agalliu, I., McMahon, A. P. and Jessell, T. M. (2009). Motor neurons with axial muscle projections specified by Wnt4/5 signaling. *Neuron* **61**, 708-720.

Allan, D. W. and Greer, J. J. (1997). Embryogenesis of the phrenic nerve and diaphragm in the fetal rat. *J. Comp. Neurol.* **382**, 459-468.

Arber, S., Han, B., Mendelsohn, M., Smith, M., Jessell, T. M. and Sockanathan, S. (1999). Requirement for the homeobox gene Hb9 in the consolidation of motor neuron identity. *Neuron* **23**, 659-674.

Babiuk, R. P., Zhang, W., Clugston, R., Allan, D. W. and Greer, J. J. (2003). Embryological origins and development of the rat diaphragm. *J. Comp. Neurol.* **455**, 477-487.

Batista, M. F., Jacobstein, J. and Lewis, K. E. (2008). Zebrafish V2 cells develop into excitatory CiD and Notch signalling dependent inhibitory VeLD interneurons. *Dev. Biol.* **322**, 263-275.

Bello, S. M., Millo, H., Rajebhosale, M. and Price, S. R. (2012). Catenin-dependent cadherin function drives divisional segregation of spinal motor neurons. *J. Neurosci.* **32**, 490-505.

Bermingham, J. R., Jr, Scherer, S. S., O'Connell, S., Arroyo, E., Kalla, K. A., Powell, F. L. and Rosenfeld, M. G. (1996). Tst-1/Oct-6/SCIP regulates a unique step in peripheral myelination and is required for normal respiration. *Genes Dev.* **10**, 1751-1762.

Bondue, A., Tännler, S., Chiapparo, G., Chabab, S., Ramialison, M., Paulissen, C., Beck, B., Harvey, R. and Blanpain, C. (2011). Defining the earliest step of cardiovascular progenitor specification during embryonic stem cell differentiation. *J. Cell Biol.* **192**, 751-765.

Briscoe, J., Pierani, A., Jessell, T. M. and Ericson, J. (2000). A homeodomain protein code specifies progenitor cell identity and neuronal fate in the ventral neural tube. *Cell* **101**, 435-445.

Champagnat, J., Morin-Surun, M. P., Fortin, G. and Thoby-Brisson, M. (2009). Developmental basis of the rostro-caudal organization of the brainstem respiratory rhythm generator. *Philos. Trans. R. Soc. B* **364**, 2469-2476.
Dasen, J. S., Liu, J. P. and Jessell, T. M. (2003). Motor neuron columnar fate imposed by sequential phases of Hox-c activity. *Nature* **425**, 926-933.
Dasen, J. S., Tice, B. C., Brenner-Morton, S. and Jessell, T. M. (2005). A Hox regulatory network establishes motor neuron pool identity and target-muscle connectivity. *Cell* **123**, 477-491.
Dasen, J. S., De Camilli, A., Wang, B., Tucker, P. W. and Jessell, T. M. (2008). Hox repertoires for motor neuron diversity and connectivity gated by a single accessory factor, FoxP1. *Cell* **134**, 304-316.
De Strooper, B., Annaert, W., Cupers, P., Saftig, P., Craessaerts, K., Mumm, J. S., Schroeter, E. H., Schrijvers, V., Wolfe, M. S., Ray, W. J. et al. (1999). A presenilin-1-dependent gamma-secretase-like protease mediates release of Notch intracellular domain. *Nature* **398**, 518-522.
Del Barrio, M. G., Taveira-Marques, R., Muroyama, Y., Yuk, D. I., Li, S., Wines-Samuelson, M., Shen, J., Smith, H. K., Xiang, M., Rowitch, D. et al. (2007). A regulatory network involving Foxn4, Mash1 and delta-like 4/Notch1 generates V2a and V2b spinal interneurons from a common progenitor pool. *Development* **134**, 3427-3436.
Demireva, E. Y., Shapiro, L. S., Jessell, T. M. and Zampieri, N. (2011). Motor neuron position and topographic order imposed by β- and γ-catenin activities. *Cell* **147**, 641-652.
Dias, T. B., Yang, Y. J., Ogai, K., Becker, T. and Becker, C. G. (2012). Notch signaling controls generation of motor neurons in the lesioned spinal cord of adult zebrafish. *J. Neurosci.* **32**, 3245-3252.
Fortin, G. and Thoby-Brisson, M. (2009). Embryonic emergence of the respiratory rhythm generator. *Respir. Physiol. Neurobiol.* **168**, 86-91.
Hirano, S., Yan, Q. and Suzuki, S. T. (1999). Expression of a novel protocadherin, OL-protocadherin, in a subset of functional systems of the developing mouse brain. *J. Neurosci.* **19**, 995-1005.
Hirasawa, T. and Kuratani, S. (2013). A new scenario of the evolutionary derivation of the mammalian diaphragm from shoulder muscles. *J. Anat.* **222**, 504-517.
Howe, J. R., Skryabin, B. V., Belcher, S. M., Zerillo, C. A. and Schmauss, C. (1995). The responsiveness of a tetracycline-sensitive expression system differs in different cell lines. *J. Biol. Chem.* **270**, 14168-14174.
Iacovino, M., Bosnakovski, D., Fey, H., Rux, D., Bajwa, G., Mahen, E., Mitanoska, A., Xu, Z. and Kyba, M. (2011). Inducible cassette exchange: a rapid and efficient system enabling conditional gene expression in embryonic stem and primary cells. *Stem Cells* **29**, 1580-1588.
Jung, H., Lacombe, J., Mazzoni, E. O., Liem, K. F., Jr, Grinstein, J., Mahony, S., Mukhopadhyay, D., Gifford, D. K., Young, R. A., Anderson, K. V. et al. (2010). Global control of motor neuron topography mediated by the repressive actions of a single hox gene. *Neuron* **67**, 781-796.
Lacombe, J., Hanley, O., Jung, H., Philippidou, P., Surmeli, G., Grinstein, J. and Dasen, J. S. (2013). Genetic and functional modularity of Hox activities in the specification of limb-innervating motor neurons. *PLoS Genet.* **9**, e1003184.
Lance-Jones, C. and Landmesser, L. (1980). Motoneurone projection patterns in the chick hind limb following early partial reversals of the spinal cord. *J. Physiol.* **302**, 581-602.
Li, X. J., Hu, B. Y., Jones, S. A., Zhang, Y. S., Lavaute, T., Du, Z. W. and Zhang, S. C. (2008). Directed differentiation of ventral spinal progenitors and motor neurons from human embryonic stem cells by small molecules. *Stem Cells* **26**, 886-893.
Liu, J. P., Laufer, E. and Jessell, T. M. (2001). Assigning the positional identity of spinal motor neurons: rostrocaudal patterning of Hox-c expression by FGFs, Gdf11, and retinoids. *Neuron* **32**, 997-1012.
Marshall, H., Nonchev, S., Sham, M. H., Muchamore, I., Lumsden, A. and Krumlauf, R. (1992). Retinoic acid alters hindbrain Hox code and induces transformation of rhombomeres 2/3 into a 4/5 identity. *Nature* **360**, 737-741.
Miles, G. B., Yohn, D. C., Wichterle, H., Jessell, T. M., Rafuse, V. F. and Brownstone, R. M. (2004). Functional properties of motoneurons derived from mouse embryonic stem cells. *J. Neurosci.* **24**, 7848-7858.
Osumi, N. and Inoue, T. (2001). Gene transfer into cultured mammalian embryos by electroporation. *Methods* **24**, 35-42.
Peljto, M. and Wichterle, H. (2011). Programming embryonic stem cells to neuronal subtypes. *Curr. Opin. Neurobiol.* **21**, 43-51.
Peljto, M., Dasen, J. S., Mazzoni, E. O., Jessell, T. M. and Wichterle, H. (2010). Functional diversity of ESC-derived motor neuron subtypes revealed through intraspinal transplantation. *Cell Stem Cell* **7**, 355-366.
Pellerin, I., Schnabel, C., Catron, K.M. and Abate, C. (1994). Hox proteins have different affinities for a consensus DNA site that correlate with the positions of their genes on the hox cluster. *Mol. Cell. Biol.* **14**, 4532-4545.
Peng, C. Y., Yajima, H., Burns, C. E., Zon, L. I., Sisodia, S. S., Pfaff, S. L. and Sharma, K. (2007). Notch and MAML signaling drives Scl-dependent interneuron diversity in the spinal cord. *Neuron* **53**, 813-827.
Perry, S. F., Similowski, T., Klein, W. and Codd, J. R. (2010). The evolutionary origin of the mammalian diaphragm. *Respir. Physiol. Neurobiol.* **171**, 1-16.
Personius, K. E., Chang, Q., Mentis, G. Z., O'Donovan, M. J. and Balice-Gordon, R. J. (2007). Reduced gap junctional coupling leads to uncorrelated motor neuron firing and precocious neuromuscular synapse elimination. *Proc. Natl. Acad. Sci. USA* **104**, 11808-11813.
Philippidou, P., Walsh, C. M., Aubin, J., Jeannotte, L. and Dasen, J. S. (2012). Sustained Hox5 gene activity is required for respiratory motor neuron development. *Nat. Neurosci.* **15**, 1636-1644.
Price, S. R., De Marco Garcia, N. V., Ranscht, B. and Jessell, T. M. (2002). Regulation of motor neuron pool sorting by differential expression of type II cadherins. *Cell* **109**, 205-216.
Rousso, D. L., Gaber, Z. B., Wellik, D., Morrisey, E. E. and Novitch, B. G. (2008). Coordinated actions of the forkhead protein Foxp1 and Hox proteins in the columnar organization of spinal motor neurons. *Neuron* **59**, 226-240.
Sabharwal, P., Lee, C., Park, S., Rao, M. and Sockanathan, S. (2011). GDE2 regulates subtype-specific motor neuron generation through inhibition of Notch signaling. *Neuron* **71**, 1058-1070.
Schroeder, T., Kohlhof, H., Rieber, N. and Just, U. (2003). Notch signaling induces multilineage myeloid differentiation and up-regulates PU.1 expression. *J. Immunol.* **170**, 5538-5548.
Sharma, K., Sheng, H. Z., Lettieri, K., Li, H., Karavanov, A., Potter, S., Westphal, H. and Pfaff, S. L. (1998). LIM homeodomain factors Lhx3 and Lhx4 assign subtype identities for motor neurons. *Cell* **95**, 817-828.
Sockanathan, S. and Jessell, T. M. (1998). Motor neuron-derived retinoid signaling specifies the subtype identity of spinal motor neurons. *Cell* **94**, 503-514.
Soundararajan, P., Miles, G. B., Rubin, L. L., Brownstone, R. M. and Rafuse, V. F. (2006). Motoneurons derived from embryonic stem cells express transcription factors and develop phenotypes characteristic of medial motor column neurons. *J. Neurosci.* **26**, 3256-3268.
Spandidos, A., Wang, X., Wang, H. and Seed, B. (2010). PrimerBank: a resource of human and mouse PCR primer pairs for gene expression detection and quantification. *Nucleic Acids Res.* **38**, D792-D799.
Sürmeli, G., Akay, T., Ippolito, G. C., Tucker, P. W. and Jessell, T. M. (2011). Patterns of spinal sensory-motor connectivity prescribed by a dorsoventral positional template. *Cell* **147**, 653-665.
Thaler, J., Harrison, K., Sharma, K., Lettieri, K., Kehrl, J. and Pfaff, S. L. (1999). Active suppression of interneuron programs within developing motor neurons revealed by analysis of homeodomain factor HB9. *Neuron* **23**, 675-687.
Tsuchida, T., Ensini, M., Morton, S. B., Baldassare, M., Edlund, T., Jessell, T. M. and Pfaff, S. L. (1994). Topographic organization of embryonic motor neurons defined by expression of LIM homeobox genes. *Cell* **79**, 957-970.
West, B. E., Parker, G. E., Savage, J. J., Kiratipranon, P., Toomey, K. S., Beach, L. R., Colvin, S. C., Sloop, K. W. and Rhodes, S. J. (2004). Regulation of the follicle-stimulating hormone beta gene by the LHX3 LIM-homeodomain transcription factor. *Endocrinology* **145**, 4866-4879.
Wichterle, H., Lieberam, I., Porter, J. A. and Jessell, T. M. (2002). Directed differentiation of embryonic stem cells into motor neurons. *Cell* **110**, 385-397.

Supplementary Materials and Methods

Mouse strains

Mice carrying the *Hb9::GFP* reporter transgene are as described (Wichterle et al., 2002). Animals were housed either in the Columbia University Animal Facility (*Hb9::GFP*) or in the KCL Biological Services Unit (CD-1) and handled according to institutional guidelines.

Retrograde labelling and isolation of phrenic neurons

Hb9::GFP transgenic embryos were harvested at E11.5, cervical/thoracic trunks dissected out and placed on silicone-coated Petri dishes in DMEM/F12 medium (Invitrogen) supplemented with 1× penicillin/streptomycin (Invitrogen). For phrenic nerve backfills, the embryonic explants were oriented ventral side up and held in place with insect needles. The phrenic nerve was bilaterally cut in the thoracic cavity with Lumsden scissors (Bio-Rad) under a fluorescence dissection microscope, and the retrograde tracer [3K lysine-fixable tetramethylrhodamine/biotin-dextran (Invitrogen), 12% in PBS] was injected with a glass capillary directly into the lesions. The embryo trunk explants were cultured for 2 hours in DMEM/F12 in an oxygenated bath at 35°C. Following the culture, spinal cord segments C3-C5 were excised from the explants and dissociated with papain (Worthington). TMR^+ GFP^+ phrenic neurons and TMR^- GFP^+ non-phrenic MNs were sorted separately by with a Beckman-Coulter Altra flow cytometer (Fig. 1), spun down and snap frozen in liquid nitrogen. In a second set of experiments, the embryo explants were placed dorsal side up, LMC neurons were retrogradely labelled through the radial nerve and then sorted using the same methodology. At least 1500 sorted MNs were used for each array analysis. Throughout this study, spinal cord segments are numbered according to the ventral roots that emerge from them.

Introduction of MN reporter genes into ESCs

A transgenic mouse ESC line based on A2lox.Cre ESCs (Iacovino et al., 2011) was established by Lipofectamine 2000 (Invitrogen)-mediated transfection of a MN-specific reporter transgene comprising the 9 kb 5′ upstream region of the murine *Hb9* gene (Arber et al., 1999), followed by a 5′ splice substrate (Choi et al., 1991), a human fusion gene of a C-terminally

truncated human *CD2* gene (Sawada et al., 1994) and eGFP, a bovine GH poly(A) signal and a hygromycin resistance cassette. Resistant ESC clones were selected with 150 µg/ml hygromycin on the hygro-resistant, mitomycin-C-treated mouse embryonic fibroblasts (PMEF-HL, Millipore), picked, expanded and then screened for MN-specific CD2-GFP expression by *in vitro* differentiation, followed by immunohistochemistry. Clone A2lox.Cre/Hb9::CD2GFP#H4 (HC2G#H4) was selected for subsequent experiments (this ESC clone was generated by E. O. Mazzoni and I.L.). To produce an ESC clone that would specifically express the protease-resistant surface marker human CD14 in MNs, a bacterial artificial chromosome (BAC) construct based on a BAC carrying the entire *Hb9* locus (RP24-351I23, CHORI) was generated (supplementary material Fig. S1). We used recombineering (Liu et al., 2003) to (1) replace the lox511 site in the pTARBAC1 vector backbone with a spectinomycin resistance cassette; (2) replace the wild-type loxP site in the vector backbone with a tol2L-Amp-tol2R transposon cassette (Suster et al., 2009); (3) insert a 5' splice substrate and a CD14-IRES-GFP-pA expression cassette, followed by a FRT-zeo-FRT resistance marker, into the first exon of the *Hb9* gene, replacing the endogenous start codon. 10 µg of the Hb9::CD14-I-GFP/FRT-zeo BAC construct and 20 µg of pCAGGS-Tol2-TP transposase expression vector (Kawakami and Noda, 2004) were co-electroporated into A2lox.Cre ESCs using a XCell GenePulser (Bio-Rad) and the following settings: 'exponential mode', 240 V, 500 µF, 4 mm cuvettes. Recombinant ESC clones were selected with 25 µg/ml zeocin (Invitrogen) on mitomycin-C-treated mouse embryonic fibroblasts, picked, expanded and then screened for MN-specific CD14/GFP expression by *in vitro* differentiation, followed by immunohistochemistry. Clone A2lox.Cre/Hb9::CD14-IRES-GFP#E3 (H14IG#E3) was selected for subsequent experiments. To generate additional MN-reporter ESC lines on a wild-type (129/ola) background, we transfected Hb9::CD14-IRES-GFP/FRT-neo version of the BAC construct and the Tol2 transposase expression vector into IB10 ESCs (Robanus-Maandag et al., 1998) and isolated clones as described above, using 350 µg/ml G418 (Invitrogen) to select recombinant clones. Clone Hb9::CD14-IRES-GFP#13 (H14IG#13) was used for subsequent experiments.

ESC culture and differentiation

Mouse ESCs were grown on mitomycin-C-treated mouse embryonic fibroblasts (PMEF-NL, Millipore) in knockout DMEM medium (Invitrogen) supplemented with 15% FBS

(Hyclone), 1% non-essential amino acids (NEAA; Invitrogen), 2 mM L-glutamine (Invitrogen), 10 nM PD173074 (FGF/VEGF receptor tyrosine kinase inhibitor; Tocris Scientific), 0.1 mM 2-mercaptoethanol (Sigma), 1:500 dilution of LIF supernatant (generated in COS7 cells with pCAGGS-LIF; the vector was kindly provided by A. Smith), 1% EmbryoMax ES Cell Qualified Nucleosides (Millipore), 5 μg/ml plasmocin (Invivogen) and 1× penicillin/streptomycin (Invitrogen). MN differentiation from ESCs was performed as described (Wichterle and Peljto, 2008) with minor modifications. ESC colonies were dissociated with 0.25% trypsin (Invitrogen) and grown in suspension in uncoated plastic dishes, where they formed EBs. In the first 2 days, EBs were cultured in ADFNK medium [Advanced-DMEM/F12 (Invitrogen) and Neurobasal medium (Invitrogen) mixed at 1:1 ratio supplemented with 2 mM L-glutamine, 0.1 mM 2-mercaptoethanol (Sigma), 10% knockout serum replacement (Invitrogen) and 1× penicillin/streptomycin]. For the subsequent 3 days the EBs were cultured in ADFNK medium supplemented with 1 μM retinoic acid (Sigma) and 0.5 μM smoothened agonist (SAG; Merck). At day 5 of differentiation, ESC-MNs were purified by MACS. Some experiments analysing the influence of Notch signalling on MN populations were performed by adding γ-secretase inhibitors LY411575 (Stemgent; 0.2 μM) or DAPT (Sigma; 10 μM) on day 2 of differentiation.

MACS isolation of ESC-MNs

EB cultures were harvested at day 5 of differentiation. Then: (1) HC2G#H4 EBs washed twice in PBS and dissociated with Liberase-DL (Roche) supplemented with 10 U/ml DNaseI (Roche) for 15 minutes at 37°C; or (2) H14IG#E3 EBs were washed in L15 medium twice and dissociated with Accumax (Millipore) for 15 minutes at 37°C. The cell aggregates were broken into single cells by pipetting up and down and washed three times (1200 rpm, 4 minutes) with L15 medium supplemented with 10 U/ml DNaseI. The cell pellet was then resuspended in 2 ml MACS buffer [PBS supplemented with 0.5% BSA (Sigma) and 10 U/ml DNaseI] and passed through a 40 μm nylon strainer (BD). The cells were centrifuged at 1200 rpm for 4 minutes and resuspended in 200 μl MACS buffer containing 20 μg/ml mouse anti-human CD2 antibody (UMCD2, Santa Cruz) or 5 μg/ml mouse anti-human CD14 (26ic, ATCC; or UCHM1, AbD Serotec). Antibody incubation was conducted at 10°C for 15 minutes. The cells were washed and then incubated with goat anti-mouse IgG MicroBeads (Miltenyi) diluted 1:10 in MACS buffer.

After the secondary antibody incubation the cells were washed again, resuspended in 600 µl MACS buffer and applied to a MS magnetic column mounted in an OctoMACS magnet (Miltenyi). The columns were washed three times with 500 µl MACS buffer, and the positive fraction eluted with 1 ml MACS buffer, following the manufacturer's instructions. Magnetically sorted HC2G#H4 or H14IG#E3 cells contained a 90-95% pure population of MNs. Owing to the presence of the protease-resistant surface receptor CD14, clone H14IG#E3 yields ~10 times more MACS-sorted ESC-MNs than clone HC2G#H4.

Doxycycline-inducible ESC lines

PN-specific transcription factor cDNAs (supplementary material Table S1) containing the complete open reading frames were subcloned into p2lox-EGFP (Iacovino et al., 2011), p2lox-gateway (Mazzoni et al., 2011) or p2lox-TRE (Bondue et al., 2011). The p2lox plasmids containing candidate gene were either transfected with pPGK-Cre (Buch et al., 2002) by lipofection (2 µg p2lox + 0.5 µg pPGK-Cre; Lipofectamine 2000, Invitrogen) or electroporated (5-10 µg p2lox) into HC2G#H4 or H14IG#E3 ESCs. Prior to transfection, the ESCs were induced to express Cre recombinase by adding 1 µg/ml doxycycline (DOX; Sigma) to the cultures for 18 hours. Recombinant clones were selected on ESC medium supplemented with 350 µg/ml G418 (Invitrogen) for 10 days. The resistant clones were individually picked, expanded and frozen (supplementary material Table S2). Each clone was further screened by *in situ* hybridisation or immunohistochemistry to confirm inducible candidate gene expression in response to DOX.

When we considered which wild-type population of ESC-MNs to use as a baseline for our GOF screen, we unexpectedly observed that the transcriptional pattern in DOX-induced parental A2lox.Cre/*Hb9::CD14-IRES-GFP* ESC-MNs is skewed towards a pattern associated with DNA damage (supplementary material Fig. S2). The most likely explanation is that the parental ESC line, but not subclones derived from it, carry a DOX-inducible *Cre* DNA recombinase transgene (Iacovino et al., 2011). A DNA damage response is linked with Cre expression in mammalian cells (Loonstra et al., 2001; Silver and Livingston, 2001), and therefore we decided to use ESC-MNs expressing a YFP transgene (iYFP) as the baseline population.

Induction of candidate genes in ESC-MNs

ESC-MNs carrying DOX-inducible phrenic candidate genes were enriched by MACS from dissociated EBs on day 5 of differentiation and plated at density of 6×10^5 cells/cm^2 on Permanox slides (Nunc) coated with growth factor reduced Matrigel (BD Biosciences). The ESC-MNs were cultured in ADFNK supplemented with 10 ng/ml mouse Gdnf (Peprotech) and DOX (1 μg/ml) for 30 hours. In some experiments, iNICD ESC-MNs were induced with DOX for only the last 10 hours of the culture. iNERT ESC-MNs were induced for either 30 hours or the last 10 hours of the culture with 1 μg/ml DOX and 100 nM 4-hydroxytamoxifen (4HT; Sigma). Total RNA was isolated using the Microprep RNA Extraction Kit (Stratagene) or the PureLink RNA Mini Kit (Ambion) according to the manufacturer's instructions. RNA integrity and purity were determined using an electrophoresis bioanalyzer (2100 Agilent Bioanalyzer) at the Genomic Centre, KCL, London. For each genotype, ESC-MNs derived from two independent ESC subclones were analysed.

Microarray analysis

When primary MNs sorted by flow cytometry were studied, mRNA was amplified using the Ovation pico RNA Amplification kit (Nugen) prior to probe synthesis. The cRNA/mRNA was then converted to single-stranded DNA, labelled and hybridised to GeneChip Mouse Genome 430 2.0 arrays (Affymetrix) (primary MNs) or GeneChip Mouse Gene 1.0 ST arrays (ESC-MNs) according to the manufacturer's instructions. Primary MNs were processed by the array facility at the MRC Centre for Developmental Neurobiology (KCL) and ESC-MNs were processed by the Genomics Centre (KCL). Primary MNs samples were normalised using both RMA and VSN algorithms implemented in Bioconductor (affy and vsn packages) (Gautier et al., 2004; Gentleman et al., 2004; Huber et al., 2002). For both normalisations, differential expression was computed using Limma (Smyth, 2005), between each primary MN subset and the mean expression over all samples. Probes sets that mapped to more than one gene were excluded from the analysis. Differential expression values were discretized to –1 (when the gene was significantly downregulated in both normalisations, when measured by posterior log-of-odds greater than 0), +1 (when it was upregulated in both normalisations) and 0 otherwise. These discretized values were then averaged over all probe sets reporting a single gene, and genes were classified according to their discretized expression patterns. Phrenic genes were scored based on

the comparison of differentially expressed genes between phrenic neurons, non-phrenic MNs derived from segments C3-C5, and radial LMC neurons. The ESC-MNs dataset was normalised using RMA (oligo package) (Carvalho and Irizarry, 2010), and expression values were corrected for batch effects using combat (Johnson et al., 2007). Lower quality probe sets (low number of probes, probe sets mapping more than one gene) were excluded from further processing. Expression values were averaged over replicated conditions, and differential expression was called when the average expression was two times higher or lower than the average expression reported in the ESC-MN controls. Microarray data are available at GEO under accession numbers GSE45809 (super series ID), GSE45807 and GSE45808 (subseries IDs).

Immunohistochemistry and *in situ* hybridisation

Embryos were fixed in 4% paraformaldehyde overnight, washed in PBS for 24 hours and then incubated in 0.1 M phosphate buffer/30% sucrose for 6 hours, all at 4°C. Embryos were embedded in OCT and sectioned on a cryostat (Zeiss) at 20 μm. Immunohistochemistry was performed as described (Lieberam et al., 2005). Antibody incubation was performed in PBS/0.1% Triton X/3% BSA using the following primary and secondary antibodies: mouse anti-Isl1/2 (4D5; DSHB), mouse anti-Lhx3 (4E12; DSHB), mouse anti-β3-tubulin (TUJ1; R&D Systems), goat anti-Pou3f1 (C-20; Santa Cruz), rabbit anti-POU3F1 (Epitomics), rabbit anti-GFP (Invitrogen), chicken anti-GFP (Invitrogen), mouse anti-ER (F-10; Santa Cruz), goat anti-Notch1 (C-20; Santa Cruz), Alexa Fluor 568 or 633 donkey anti-mouse IgG, Alexa Fluor 488, 568 or 633 donkey anti-rabbit IgG, Alexa Fluor 488 goat anti-chicken IgY (all secondary antibodies were obtained from Invitrogen). DNA counterstaining was carried out by adding 0.2 μM TOPRO3 (Invitrogen) to the secondary antibody labelling mix.

In situ hybridisation was performed as described (Lieberam et al., 2005). The following probes were used on mouse embryos: *Cdh9*, *Cdh10*, *Pcdh10*, *Pcdh11x*, *Alcam*, *Negr1*, *Synpr*, *Plxnc1*, *Ptn*, *Pappa*, *Zbtb7c*, *Hoxa1*, *Hoxa5*, *Klf5*, *Edil3*, *Vwc2*, *Vwc2l*, *Mmd2*, *Hs6st2*, *Dll4*, *Hey1*, *Isl1* and *Pou3f1*. A list of probes used to test DOX-inducible gene expression in EBs can be found in supplementary material Table S1.

Quantitative RT-PCR

RNA was isolated from cultured ESC-MNs using the PureLink RNA Mini Kit (Ambion). cDNA was synthesized with the High Capacity RNA-to-cDNA Kit (Invitrogen). Real-time qPCR reactions were prepared using the Power SYBR Green PCR Master Mix (Life Technologies/Applied Biosystems). PCR reactions were then performed in 384-well Microamp plates (Applied Biosystems) with the Prism 7000 Sequence Detection System (Applied Biosystems) at the Genomic Centre, KCL, London. Cycling conditions: 50°C, 2 minutes (×1); 95°C, 10 minutes (×1); cycle: 95°C for 15 seconds, 60°C for 30 seconds, 72°C for 30 seconds (×40). Primer sequences were obtained from the PrimerBank database (Spandidos et al., 2010) and are shown in supplementary material Table S3. The fold-change in gene expression was expressed in CT.

MN mixing assay

EBs derived from the ESC subclones iMT, iTagRFP, iCdh10 and iPcdh10 were induced with 1 μg/ml DOX on day 4, MNs were MACS-sorted on day 5, mixed 1:1 and cultured in Matrigel-coated μ-Slides VI (Ibidi) (3×10^5 cells/well) in the presence of DOX. The following combinations of genotypes were tested for their ability to segregate in mixed clusters: (1) iTagRFP/iMT, (2) iTagRFP/iPcdh10, (3) iTagRFP/iCdh10. The slides were fixed after 24 hours with 4% paraformaldehyde at room temperature for 20 minutes, washed with PBS, nuclei were visualised by staining with 0.2 μM TOPRO3 in PBS for 1 hour, and MN aggregates were imaged by confocal microscopy. GFP and RFP were detected by direct fluorescence.

Whole embryo culture (WEC)

E9.75 embryos (25-26 somite stage) obtained from timed-pregnant CD1 outbred mice were isolated from the uterus as described (Osumi and Inoue, 2001; Takahashi and Osumi, 2010), and visceral yolk sac and amnion were opened to improve oxygenation. After the preparation, the embryos were transferred into a sterile glass roller bottle containing high-glucose DMEM (Sigma) supplemented with 50% WEC-grade rat serum (Harlan US) and 0.5× penicillin/streptomycin. The culture bottles were moved to the WEC system (model RKI 10-0310, Ikemoto Scientific Technology, Tokyo, Japan), attached to rotator drum and cultured for 2 hours prior to electroporation (Takahashi and Osumi, 2010). After 2 hours, the embryos were removed from the bottles and placed dorsal side up in a cavity carved into a 6 cm Petri dish

covered with solidified 3% low melting point agarose (Sigma). Then, the roof plate of the spinal cord was punctured at segments T2-T4 using a 33G needle (TSK Laboratory, Japan). A glass capillary was inserted dorsally into the fourth ventricle and moved caudally towards the central canal, and 0.1-0.5 µl of plasmid solution (5 µg/ml, 0.02% Fast Green, in PBS) was injected by mouth pipetting into the lumen of the spinal cord. The embryo was transferred to a saline-containing bath-type electrode (CUY-520P20, Nepa Gene, Tokyo, Japan), placed such that the right side of the embryo faced the anode, and square pulses (70 V, 1 pulse/second, 50 milliseconds pulse duration, five pulses) were applied with a XCell GenePulser (Bio-Rad). The expression vector carrying pcDNA-DLL4 (Del Barrio et al., 2007) or empty control vector was mixed 4:1 with the IRES-nlsGFP derivative of the reporter plasmid pCAGGS (Niwa et al., 1991). All embryo manipulations were performed either in Tyrode's Balanced Salt Solution (TBSS) (Sigma)/0.2% BSA (embryo preparation, DNA injection) or in TBSS alone (electroporation). Following electroporation, the embryos were returned to the WEC system. Embryos were harvested 40 hours later for the analysis of Pou3f1 and Isl1/2 expression in the cervical spinal cord. Only embryos with normal morphology, a beating heart and a good blood circulation were selected for further analysis. WEC experiments were carried out under license from the UK Home Office in accordance with the Animals (Scientific Procedures) Act 1986 (Amended Regulations 2012) and following ethical approval from King's College London.

Image acquisition and analysis

Images were acquired using a Zeiss 710 confocal microscope through a 20× lens with a numerical aperture of 0.8. Optical section stacks were processed with ImageJ software (http://rsb.info.nih.gov/ij/) or ZEN software (Zeiss). Image analysis was performed in maximum intensity *z*-projections. When quantifying Pou3f1 expression in transfected WEC embryos, only pairs of sections with >15 GFP^+ cells below the dorsal margin of the motor columns on the transfected side were included in the analysis. Cell body clustering of cultured ESC-MNs was scored by near-neighbour analysis using Imaris software (Bitplane). In some experiments, the *in situ* hybridisation signal in sectioned EBs was quantified with ImageJ as pixels/area.

Antibodies

Antibody	Company	Stock Number
Mouse anti-CD14 (UCHM1)	AbD Serotec	MCA596XZ
Mouse anti-CD2 (UMCD2)	Santa Cruz	sc-65247
Goat-anti-mouse IgG microbeads	Miltenyi Biotec	130-048-401
Mouse anti-b3-Tubulin (TUJ1)	R&D Systems	MAB1195
Goat anti-Pou3f1 (C-20)	Santa Cruz	sc-11661
Rabbit anti-POU3F1	Epitomics	EP5421
Rabbit anti-GFP (IgG fraction)	Invitrogen	A11122
Chicken anti-GFP	Invitrogen	A10262
Mouse anti-ERa (F-10)	Santa Cruz	sc-8002
Goat anti-Notch1 (C-20)	Santa Cruz	sc-6014
Alexa Fluor 568 donkey anti-mouse IgG	Invitrogen	A10037
Alexa Fluor 647 donkey anti-mouse IgG	Invitrogen	A31571
Alexa Fluor 488 donkey anti-rabbit IgG	Invitrogen	A21206
Alexa Fluor 568 donkey anti-rabbit IgG	Invitrogen	A10042
Alexa Fluor 633 goat anti-rabbit IgG	Invitrogen	A21244
Alexa Fluor 488 goat anti-chicken IgY	Invitrogen	A11039

For all other antibodies, hybridomas were obtained from ATCC or DSHB as indicated in the text, and antibody protein purified from culture supernatants using Protein-G affinity chromatography.

References

Arber, S., Han, B., Mendelsohn, M., Smith, M., Jessell, T. M. and Sockanathan, S. (1999). Requirement for the homeobox gene Hb9 in the consolidation of motor neuron identity. *Neuron* **23**, 659-674.

Bondue, A., Tannler, S., Chiapparo, G., Chabab, S., Ramialison, M., Paulissen, C., Beck, B., Harvey, R. and Blanpain, C. (2011). Defining the earliest step of cardiovascular progenitor specification during embryonic stem cell differentiation. *J. Cell Biol.* **192**, 751-765.

Buch, T., Rieux-Laucat, F., Forster, I. and Rajewsky, K. (2002). Failure of HY-specific thymocytes to escape negative selection by receptor editing. *Immunity* **16**, 707-718.
Carvalho, B. S. and Irizarry, R. A. (2010). A framework for oligonucleotide microarray preprocessing. *Bioinformatics* **26**, 2363-2367.
Choi, T., Huang, M., Gorman, C. and Jaenisch, R. (1991). A generic intron increases gene expression in transgenic mice. *Mol. Cell. Biol.* **11**, 3070-3074.
Del Barrio, M. G., Taveira-Marques, R., Muroyama, Y., Yuk, D. I., Li, S., Wines-Samuelson, M., Shen, J., Smith, H. K., Xiang, M., Rowitch, D. et al. (2007). A regulatory network involving Foxn4, Mash1 and delta-like 4/Notch1 generates V2a and V2b spinal interneurons from a common progenitor pool. *Development* **134**, 3427-3436.
Gautier, L., Cope, L., Bolstad, B. M. and Irizarry, R. A. (2004). Affy-analysis of Affymetrix GeneChip data at the probe level. *Bioinformatics* **20**, 307-315.
Gentleman, R., Carey, V., Bates, D., Bolstad, B., Dettling, M., Dudoit, S., Ellis, B., Gautier, L., Ge, Y., Gentry, J. et al. (2004). Bioconductor: open software development for computational biology and bioinformatics. *Genome Biology* **5**, R80.
Huber, W., von Heydebreck, A., Sueltmann, H., Poustka, A. and Vingron, M. (2002). Variance stabilization applied to microarray data calibration and to the quantification of differential expression. *Bioinformatics* **18**, S96-S104.
Iacovino, M., Bosnakovski, D., Fey, H., Rux, D., Bajwa, G., Mahen, E., Mitanoska, A., Xu, Z. and Kyba, M. (2011). Inducible cassette exchange: a rapid and efficient system enabling conditional gene expression in embryonic stem and primary cells. *Stem Cells* **29**, 1580-1588.
Johnson, W. E., Li, C. and Rabinovic, A. (2007). Adjusting batch effects in microarray expression data using empirical Bayes methods. *Biostatistics* **8**, 118-127.
Kawakami, K. and Noda, T. (2004). Transposition of the Tol2 element, an Ac-like element from the Japanese medaka fish Oryzias latipes, in mouse embryonic stem cells. *Genetics* **166**, 895-899.
Lieberam, I., Agalliu, D., Nagasawa, T., Ericson, J. and Jessell, T. M. (2005). A Cxcl12-Cxcr4 chemokine signaling pathway defines the initial trajectory of mammalian motor axons. *Neuron* **47**, 667-679.
Liu, P., Jenkins, N. A. and Copeland, N. G. (2003). A highly efficient recombineering-based method for generating conditional knockout mutations. *Genome Res.* **13**, 476-484.
Loonstra, A., Vooijs, M., Beverloo, H. B., Allak, B. A., van Drunen, E., Kanaar, R., Berns, A. and Jonkers, J. (2001). Growth inhibition and DNA damage induced by Cre recombinase in mammalian cells. *Proc. Natl. Acad. Sci. USA* **98**, 9209-9214.
Mazzoni, E. O., Mahony, S., Iacovino, M., Morrison, C. A., Mountoufaris, G., Closser, M., Whyte, W. A., Young, R. A., Kyba, M., Gifford, D. K. et al. (2011). Embryonic stem cell-based mapping of developmental transcriptional programs. *Nat. Methods* **8**, 1056-1058.
Niwa, H., Yamamura, K. and Miyazaki, J. (1991). Efficient selection for high-expression transfectants with a novel eukaryotic vector. *Gene* **108**, 193-199.
Osumi, N. and Inoue, T. (2001). Gene transfer into cultured mammalian embryos by electroporation. *Methods* **24**, 35-42.
Robanus-Maandag, E., Dekker, M., van der Valk, M., Carrozza, M. L., Jeanny, J. C., Dannenberg, J. H., Berns, A. and te Riele, H. (1998). p107 is a suppressor of retinoblastoma development in pRb-deficient mice. *Genes Dev.* **12**, 1599-1609.

Sawada, S., Scarborough, J. D., Killeen, N. and Littman, D. R. (1994). A lineage-specific transcriptional silencer regulates CD4 gene expression during T lymphocyte development. *Cell* **77**, 917-929.
Silver, D. P. and Livingston, D. M. (2001). Self-excising retroviral vectors encoding the Cre recombinase overcome Cre-mediated cellular toxicity. *Mol. Cell* **8**, 233-243.
Smyth, G. K. (2005). Limma: linear models for microarray data. In *Bioinformatics and Computational Biology Solutions Using R and Bioconductor*, (ed. R. C. Gentleman V. J. Carey S. Dudoit R. Irizarry and W. Huber), pp. 397-420. New York: Springer.
Spandidos, A., Wang, X., Wang, H. and Seed, B. (2010). PrimerBank: a resource of human and mouse PCR primer pairs for gene expression detection and quantification. *Nucleic Acids Res.* **38**, D792-D799.
Suster, M. L., Sumiyama, K. and Kawakami, K. (2009). Transposon-mediated BAC transgenesis in zebrafish and mice. *BMC Genomics* **10**, 477.
Takahashi, M. and Osumi, N. (2010). The method of rodent whole embryo culture using the rotator-type bottle culture system. *J. Vis. Exp*. doi: 10.3791/2170.
Wichterle, H., Lieberam, I., Porter, J. A. and Jessell, T. M. (2002). Directed differentiation of embryonic stem cells into motor neurons. *Cell* **110**, 385-397.
Wichterle, H. and Peljto, M. (2008). Differentiation of mouse embryonic stem cells to spinal motor neurons. *Curr. Protoc. Stem Cell Biol.* **Chapter 1**, Unit 1H 1 1-1H 1 9.

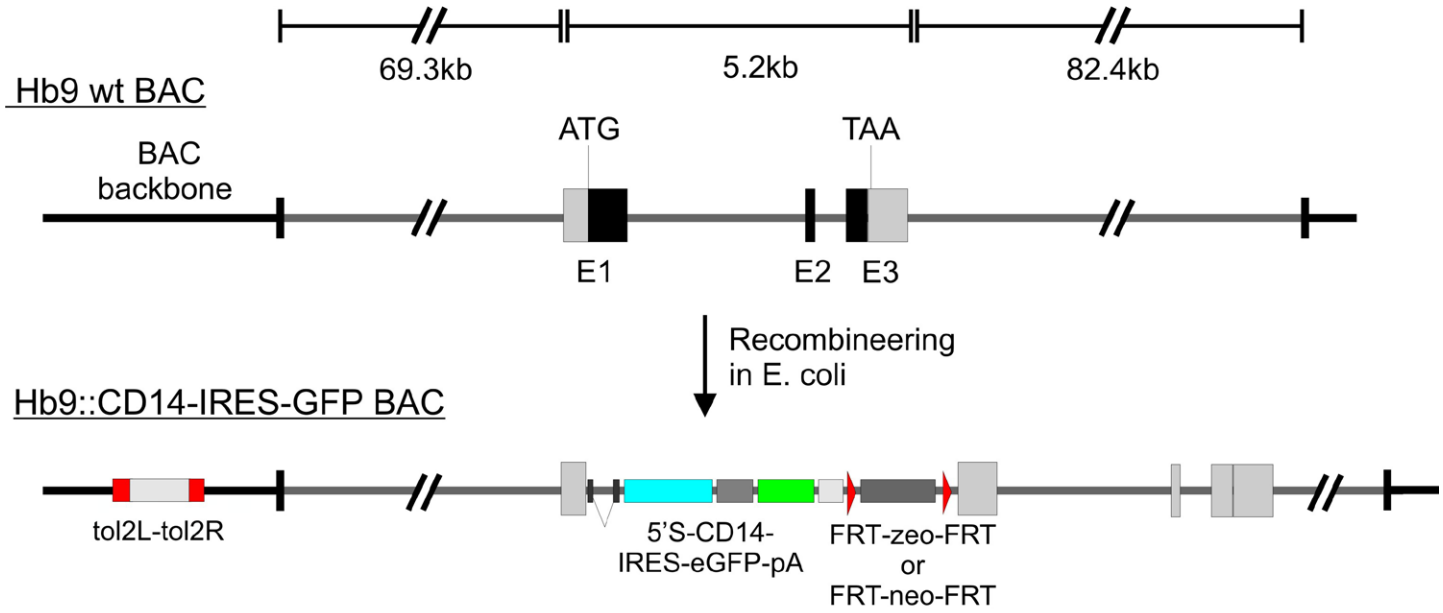

Fig. S1. BAC constructs used for the generation of Hb9::CD14-IRES-GFP transgenic ESC clones. MNs derived from these ESCs specifically express the surface protein CD14 and GFP. The Hb9::CD14-IRES-GFP/FRT-zeo-FRT construct was used to generate ESC clone H14IG#E3 one the A2lox.Cre background, the Hb9::CD14-IRES-GFP/FRT-neo-FRT variant was used to establish ESC clone H14IG#13 one a wild-type 129/ola (IB10) background. The tol2-insertion site in clone H14IG#13 was mapped close to the *Cacna1a* gene (chromosome 8.C2) by inverse PCR (Kawakami and Noda, 2004). We have been unable to identify the BAC insertion site in clone H14IG#E3.

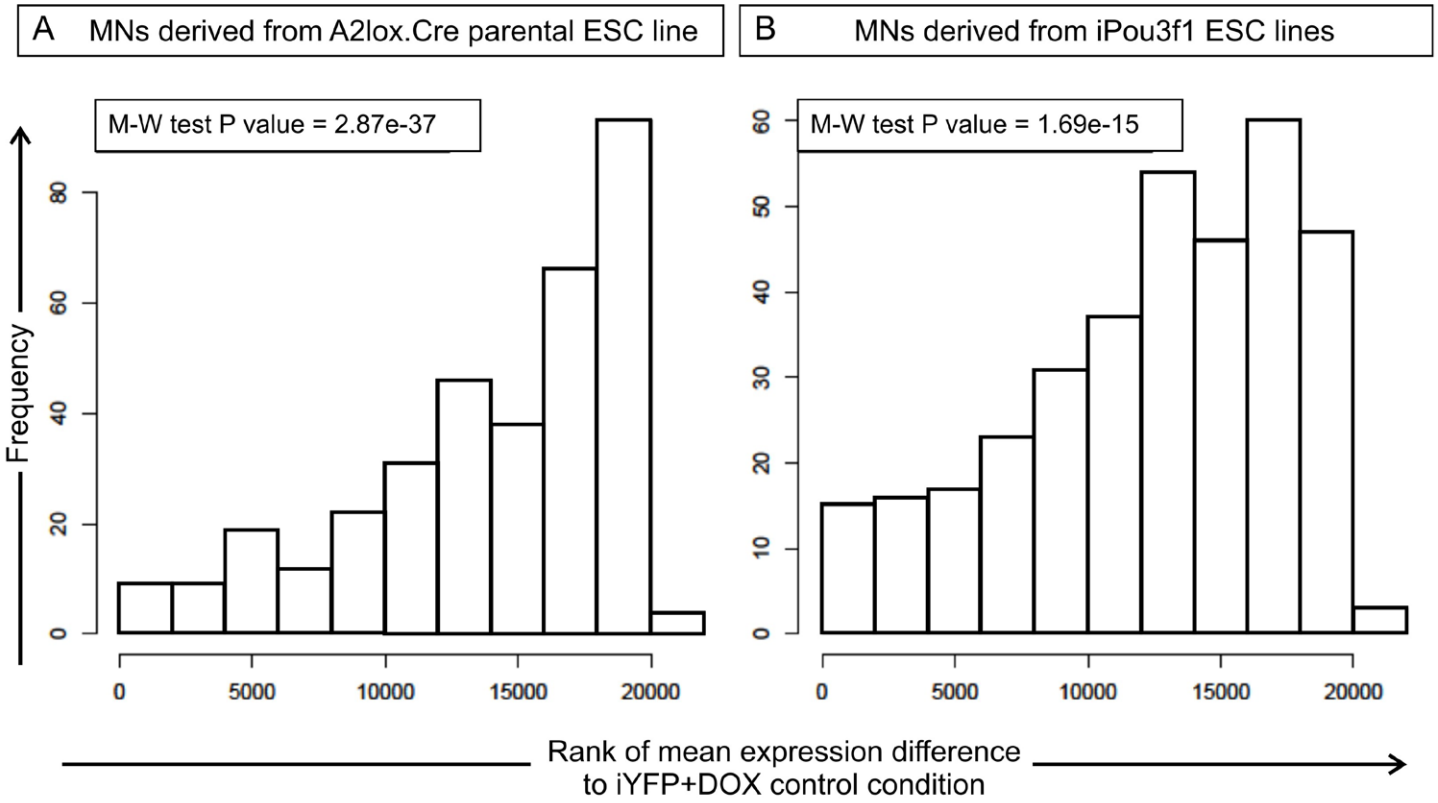

Fig. S2. DNA damage response in DOX-induced A2lox.Cre ESC-MNs. DOX-Induction of Cre recombinase expression in ESC-MNs derived from parental A2lox.Cre/H14IG#E3 ESCs elicits transcription changes related to the DNA damage response, as reported by the Mann-Whitney test over the expression difference for 349 genes annotated with the Gene Ontology term GO:0006974. (A) Distribution of 349 genes annotated with term GO:006974 in DOX-induced parental A2lox.Cre/H14IG#E3, compared to DOX-induced iYFP controls. Both ESC-MN populations were analysed in duplicates. (B) Same analysis as in A, except that iPou3f1 ESC-MNs were compared to iYFP ESC-MNs.

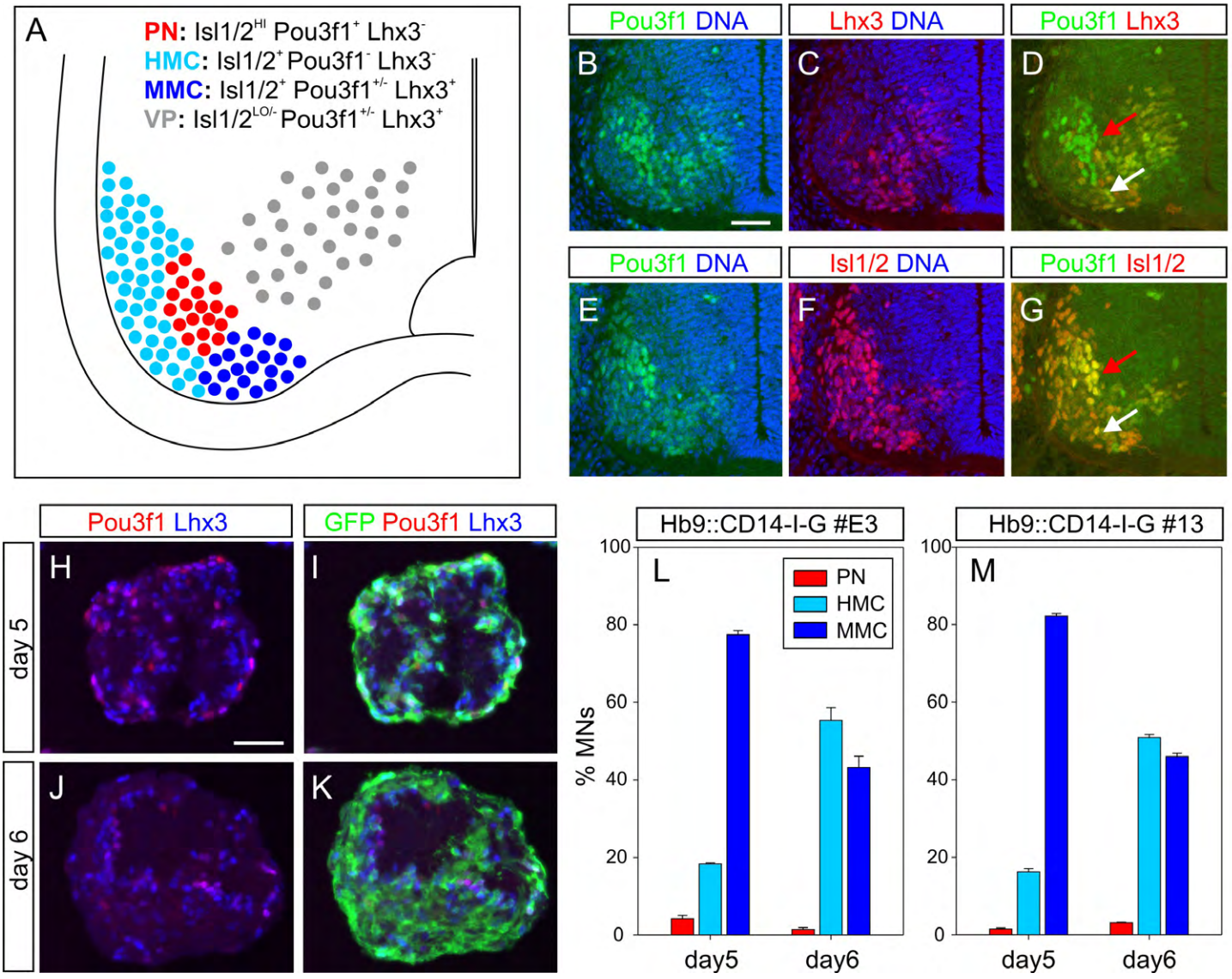

Fig. S3. ESC-MNs phenotypically resemble MMC- and HMC- but not phrenic MNs. (A) This scheme shows marker expression and anatomical position of MN subtypes in the mid-cervical spinal cord at E11.5. (B-D) Expression of Pou3f1 and the MMC-marker Lhx3, and (D-F) Pou3f1 and pan-MN marker Isl1/2 at E11.5 in the mid-cervical spinal cord. Pou3f1 protein was detected in the phrenic nucleus (red arrows) and some MNs in the lateral part of the MMC (white arrows). Scale bars 50 µm. (H-K) Expression of GFP, Lhx3 and Pou3f1 in day 5 (H, I) and day 6 (J, K) EBs derived from *Hb9::CD14-IRES-GFP* ESCs (clone H14IG#E3). (L) Percentages of HMC-like, MMC-like and phrenic neuron-like ESC-MNs in day 5 and day 6 EBs derived from ESC clone H14IG#E3. The bars represent mean values from two independent experiments +/- s.e.m. (M) Same analysis as in (L), but with EBs derived from ESC clone H14IG#13.

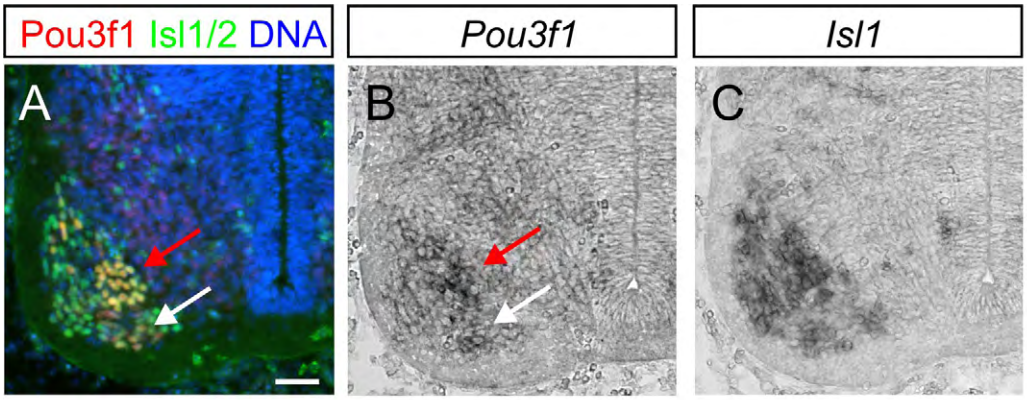

Fig. S4. Phrenic neurons and a subset of MMC neurons express both Pou3f1 protein and *Pou3f1* mRNA. (A) Pou3f1, Isl1/2 and DNA staining in the E11.5 mid-cervical spinal cord. Pou3f1 protein is found both in the PN (red arrow) and in the lateral part of the MMC (white arrow). (B) *Pou3f1* mRNA shows the same restriction to the PN (red arrow) and the lateral MMC (white arrow). (C) *Isl1* mRNA labels all MNs in the mid-cervical spinal cord.

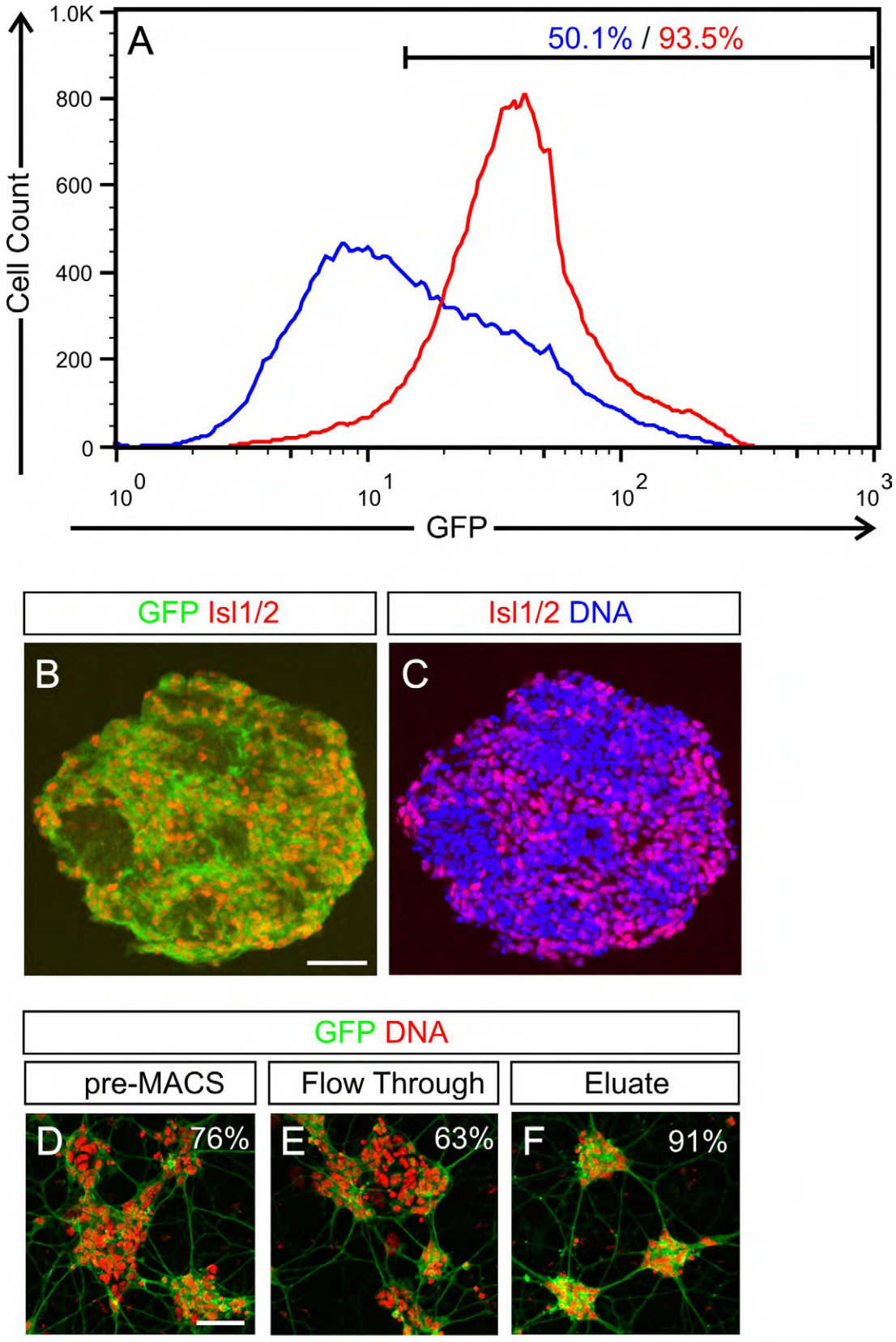

Fig. S5. Isolation and culture of *Hb9::CD2GFP* transgenic ESC-MNs. (A) Flow cytometric analysis of ESC-MNs enrichment by anti-CD2 MACS. (B, C) Cross sections through day 6 EBs. Expression of the GFP reporter correlates tightly with endogenous MN marker Isl1/2. (D, E, F) GFP-labelled MNs are enriched in overnight cultures of anti-CD2 MACS eluates (F), compared to the pre-MACS input (D) or the flow-through (E). The percentage of GFP^+ cells is indicated in the upper right corner of each image. Three representative images per condition were counted.

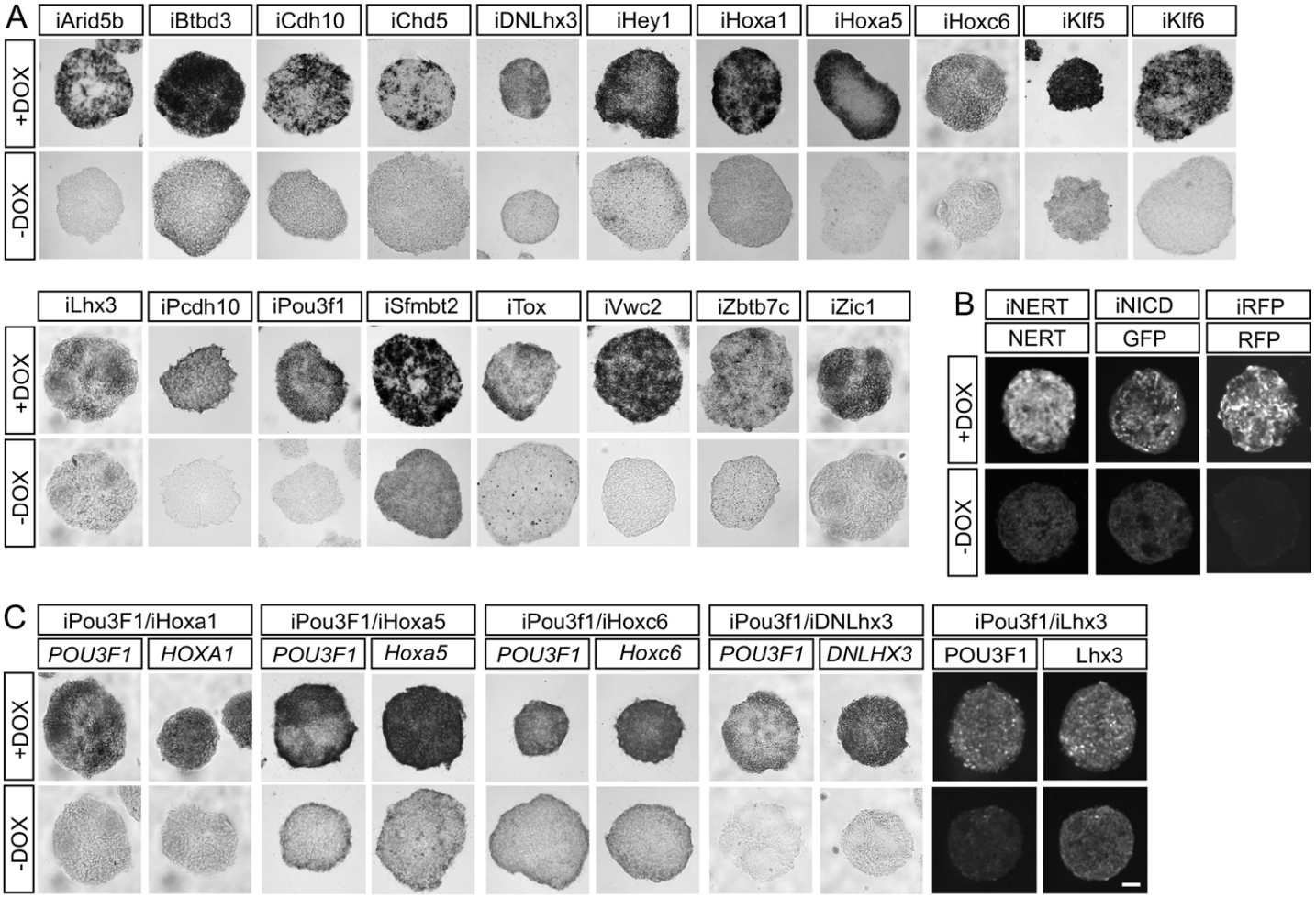

Fig. S6. Confirmation of candidate gene expression in EBs derived from A2lox subclones carrying one or two inducible transgene(s). (A) mRNA expression of candidate genes in day 6 EBs with/without DOX-induction on day 5 in EBs with single transgenes (see labels above images). (B) Protein expression of candidate genes in day 6 EBs with/without DOX-induction on day 5 in EBs with single transgenes (see labels above images). (C) Protein/mRNA expression of candidate genes in day 6 EBs with/without DOX-induction on day 5 in EBs with two transgenes (see labels above images). Scale bar 50 μm.

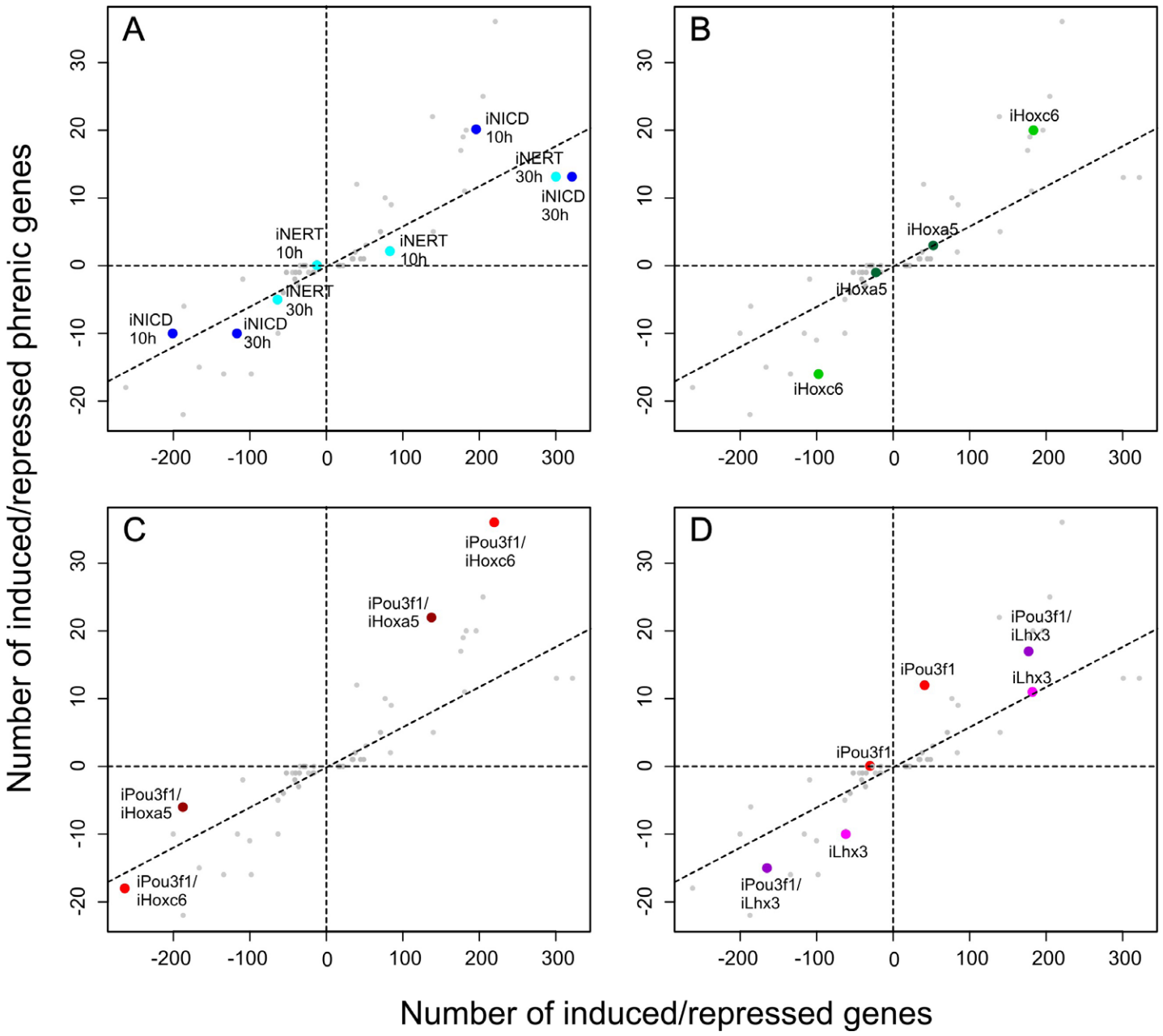

Fig. S7. Induction of PN-like transcriptional patterns by selected candidate factors in ESC-MN. These scatter plots show the same expression data as Fig. 4, except that different subsets of candidate factors are highlighted: (A) iNICD and iNERT, induced for 10 hours or 30 hours. (B) iHoxa5 and iHoxc6. (C) iPou3f1/iHoxa5 and iPou3f1/iHoxc6. (D) iPou3f1, iLhx3 and iPou3f1/iLhx3.

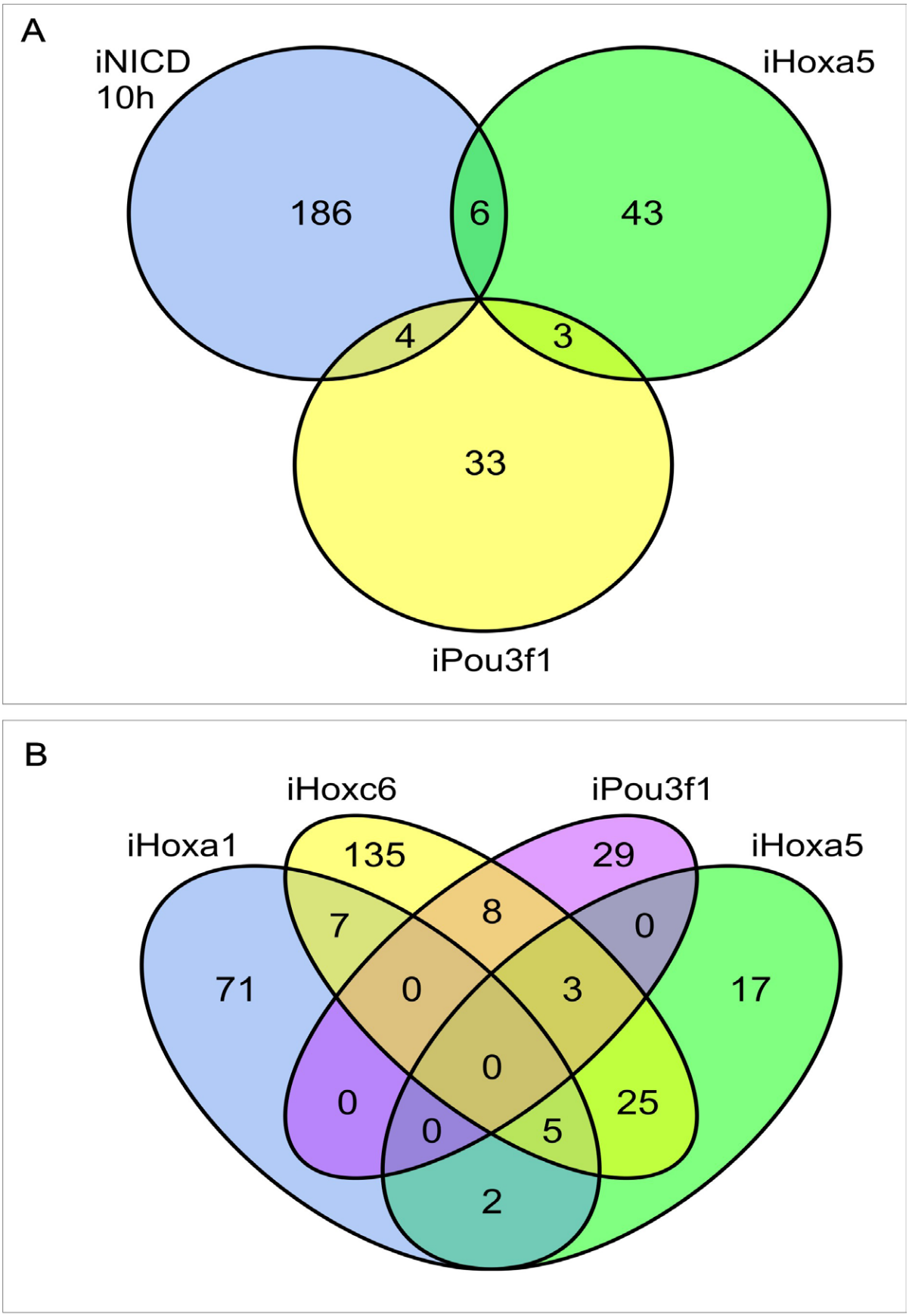

Fig. S8. Venn diagrams showing the degree of overlap between target gene sets of individual candidate PN-determinants. (A) Three-way comparison between target genes of iNICD (10 hours induction), iPou3f1 and iHoxa5 in ESC-MNs. (B) Four-way comparison between target genes of iPou3f1, iHoxc6, iHoxa5 and iHoxa1 in ESC-MNs.

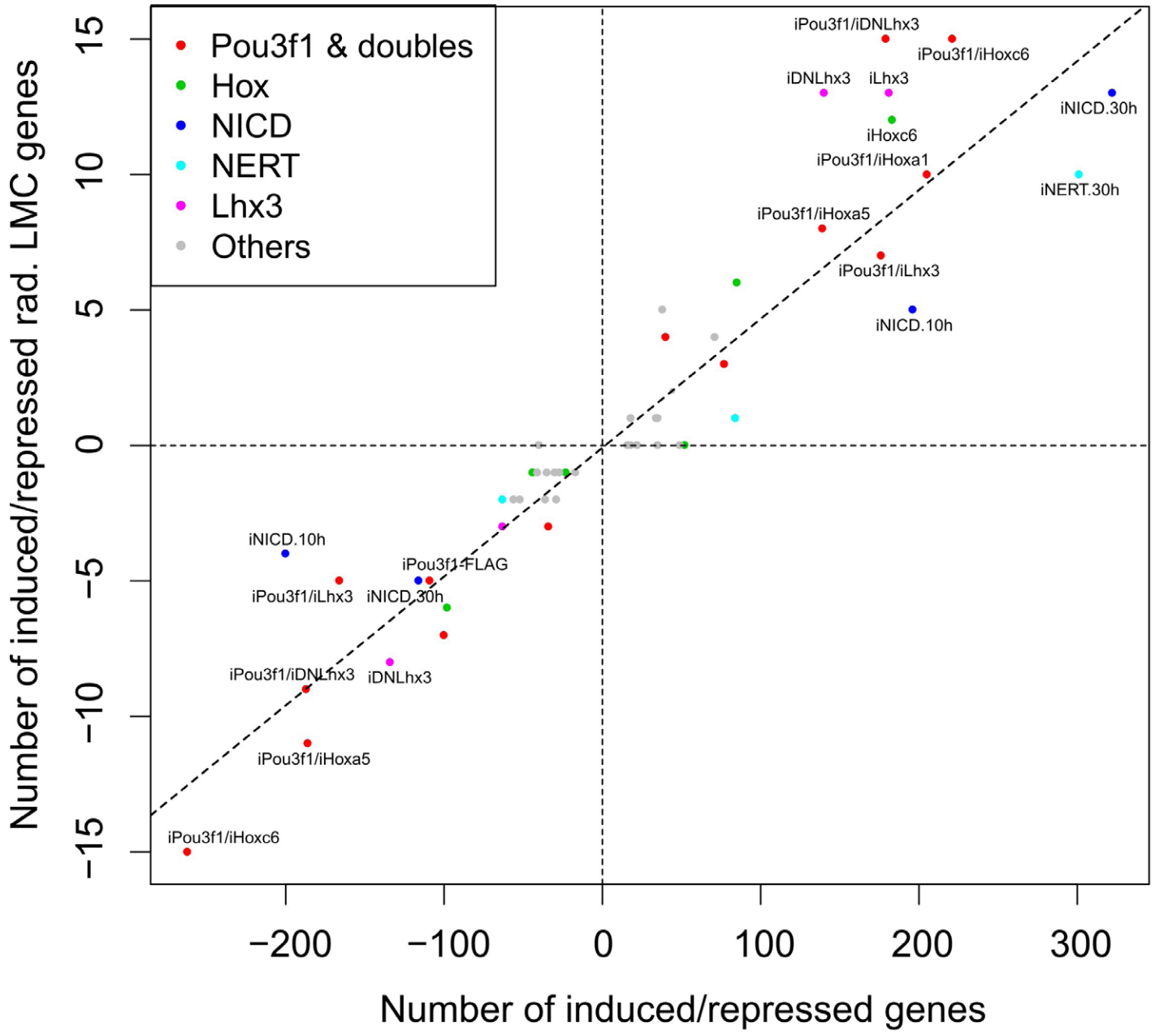

Fig. S9. Identification of transcription factors that control parts of the radial LMC-specific transcriptional pattern. MACS-sorted ESC-MNs were induced to express candidate determinants, and their transcriptional profiles were examined by Affymetrix array analysis. In the scatter plot, the number of radial LMC-specific genes induced/repressed (y-axis) is plotted against the number of all gene induced/repressed (x-axis) by a given candidate factor or combination thereof. On both axes, positive values correspond to numbers of induced genes, while negative values correspond to numbers of repressed genes. The diagonal line represents a robust fit through all the points shown, both induced and repressed.

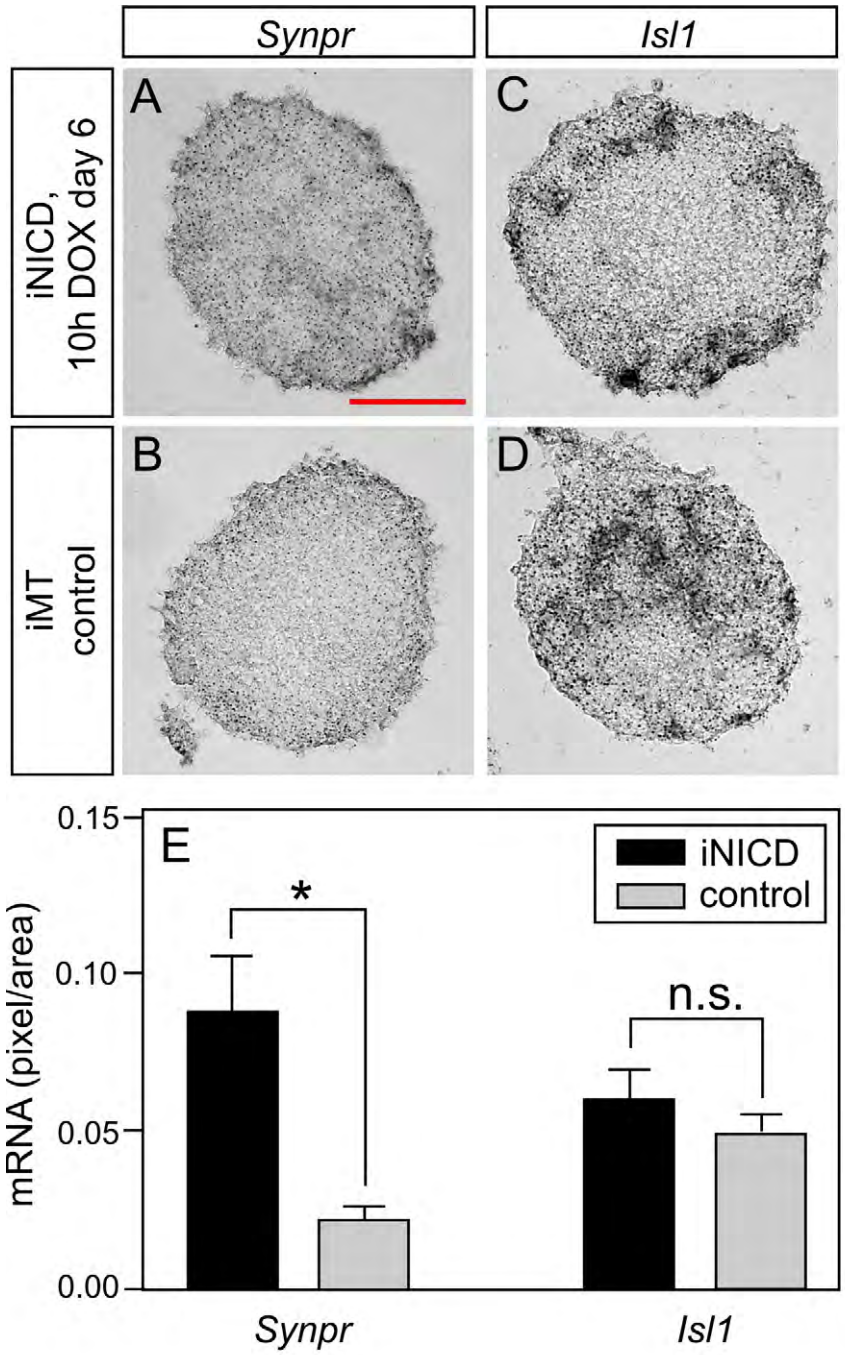

Fig. S10. NICD up-regulates the PN-marker *Synpr* in EBs. (A, B) *Synpr* mRNA expression in day 8 iNICD EBs is increased following a 10 hour pulse of DOX on day 6, compared to normal control EBs that carry a non-coding inducible transcript (iMT). Scale bar 50 µm. (C, D) *Isl1* mRNAs expression in day 8 iNICD and control EBs (same conditions as in (A, B)). (E) Quantification of gene expression levels of *Synpr* and *Isl1* mRNA in sectioned day 8 EBs. The bars represent mean values from ten EBs per condition +/- s.e.m. *$p<0.05$ (two-sample Student's *t*-test); n.s.: not significant.

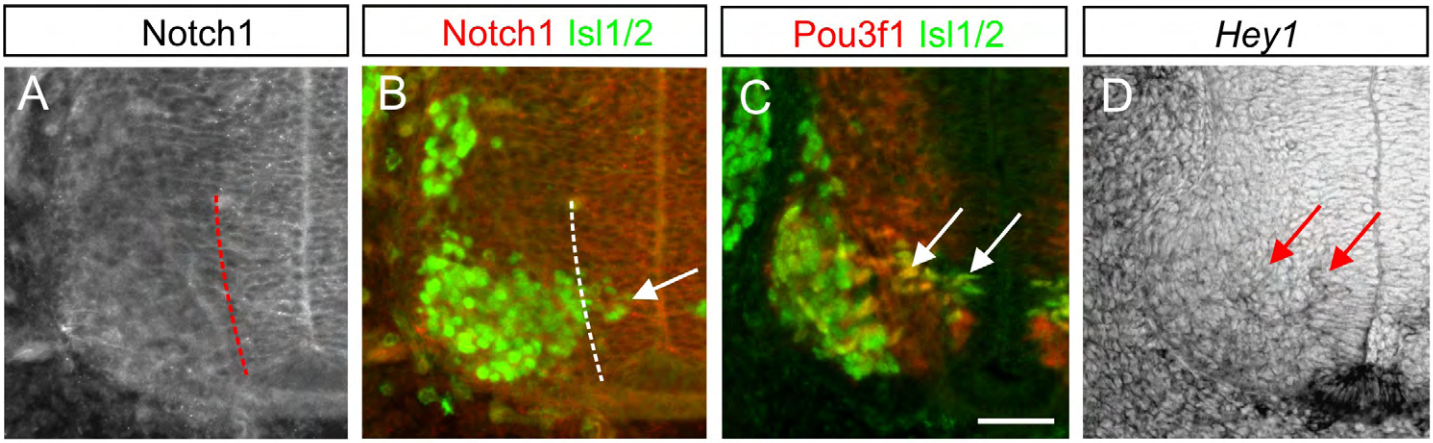

Fig. S11. Notch1 protein is present on immature MNs, and Pou3f1 expression in nascent phrenic neurons overlaps with *Hey1*. (A, B) Expression of Notch1 and the MN marker Isl1/2 proteins overlaps in mid-cervical E10.5 embryonic spinal cord (white arrow). The red/white dotted lines demarcate the boundary between Notch1-positive medial spinal cord and Notch1-low/negative lateral spinal cord. (C) Expression of Pou3f1 and Isl1/2 in mid-cervical E10.5 spinal cord. Both medial nascent Isl1/2^{+} MNs and more lateral Pou3f1^{+}Isl1/2^{+} MNs are marked (red arrows). Scale bar 50 μm. (D) Expression of *Hey1* overlaps with the positions of early post-mitotic MNs (white arrows). Images C and D show adjacent sections of the same embryo.

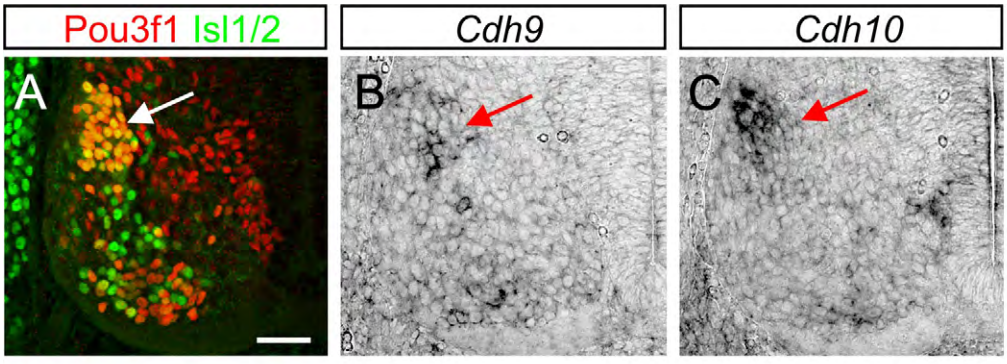

Fig. S12. Ulnar MNs share Pou3f1, *Cdh9* and *Cdh10* expression with the PN. (A) Protein expression of Pou3f1 and Isl1/2 in the E11.5 caudal brachial spinal cord (~C7 segment). Ulnar MNs express high levels of both markers and are labelled in orange (white arrow). Scale bar 50 μm. (B, C) *Cdh9* and *Cdh10* mRNAs show the same restriction to ulnar MNs (red arrows).

Table S1. List of candidate genes ectopically expressed in ESC-MNs.

Gene	Accession number	Source	Cat #	Species
ARID5B	NM_032199	Open Biosystems	OHS5894-99848148	human
Btbd3	NM_145534	Open Biosystems	MMM1013-9497834	mouse
Cdh10	NM_009865	1	n.a.	mouse
CHD5	NM_015557	Open Biosystems	OHS5893-99847976	human
DNLHX3	n.a.	2	n.a.	human
Hey1	NM_010423	Open Biosystems	MMM1013-98479373	mouse
HOXA1	NM_005522	Open Biosystems	OHS1770-9385476	human
Hoxa5	NM_010453	Open Biosystems	MMM1013-65166	mouse
Hoxc6	NM_010465	Open Biosystems	EMM1002-99864377	mouse
Klf5	NM_009769	Open Biosystems	MMM1013-64973	mouse
KLF6	NM_001300	Open Biosystems	OHS5893-99856561	human
Lhx3	NM_001039653	Open Biosystems	MMM1013-99826983	mouse
NOTCH1-ICD(ΔOP)-ERT	n.a.	3	n.a.	mouse
NOTCH1-ICD-GFP	n.a.	4	n.a.	human
Pcdh10	BC065695	Open Biosystems	MMM1013-202799110	mouse
POU3F1	NM_002699	Open Biosystems	OHS5894-99848358	human
POU3F1-FLAG	n.a.	Lieberam group	n.a.	human
SFMBT2	NM_001018039	Open Biosystems	OHS5893-99856528	human
TOX	NM_014729	Open Biosystems	OHS4559-99856692	human
Vwc2	NM_177033	Open Biosystems	MMM1013-99829278	mouse
ZBTB7C	NM_001039360	Open Biosystems	OHS5893-99856503	human
Zic1	NM_009573	Open Biosystems	MMM1013-9334882	mouse

1. Prof. Uwe Drescher, MRC Centre for Developmental Neurobiology, King's College London, London, UK.
2. Prof. Simon J. Rhodes, Stark Neurosciences Research Institute, Indiana University, Indianapolis, IN, USA.
3. Prof. Ursula Just, Biochemical Institute, Christian-Albrechts-University of Kiel, Kiel, Germany.
4. Dr Dafe A. Uwanogho, Institute of Psychiatry, King's College London, London, UK.

Table S2. List of transgenic A2lox ESC subclones used for MN differentiation. *ESC subclones iMT, iRFP, iPcdh10 and iCdh10 were only used for cell mixing experiments, but not for Affymetrix array analysis of transcriptional profiles.

DOX-inducible gene(s)	Parental ESC line	MN-specific reporter	Clones #
ARID5B	HC2G#H4	Hb9::hCD2GFP	1, 2
Btbd3	HC2G#H4	Hb9::hCD2GFP	1, 2
Cdh10*	H14IG#E3	Hb9::hCD14-IRES-GFP	3, 4
CHD5	HC2G#H4	Hb9::hCD2GFP	1, 2
DNLHX3	HC2G#H4	Hb9::hCD2GFP	1, 2
Hey1	HC2G#H4	Hb9::hCD2GFP	1, 2
HOXA1	HC2G#H4	Hb9::hCD2GFP	6, 8
Hoxa5	HC2G#H4	Hb9::hCD2GFP	1, 2
Hoxc6	HC2G#H4	Hb9::hCD2GFP	1, 2
Klf5	HC2G#H4	Hb9::hCD2GFP	7, 8
KLF6	HC2G#H4	Hb9::hCD2GFP	1, 2
Lhx3	HC2G#H4	Hb9::hCD2GFP	1, 2
MT (non-coding mock transcript)*	H14IG#E3	Hb9::hCD14-IRES-GFP	3, 4
NOTCH1-ICD(ΔOP)-ERT (NERT)	H14IG#E3	Hb9::hCD14-IRES-GFP	1, 2
NOTCH1-ICD-GFP	HC2G#H4	Hb9::hCD2GFP	1, 2
Pcdh10*	H14IG#E3	Hb9::hCD14-IRES-GFP	3, 4
POU3F1	HC2G#H4	Hb9::hCD2GFP	1, 2
POU3F1	H14IG#E3	Hb9::hCD14-IRES-GFP	1, 2
POU3F1-FLAG	H14IG#E3	Hb9::hCD14-IRES-GFP	1, 2
POU3F1 / DN-LHX3	H14IG#E3	Hb9::hCD14-IRES-GFP	1, 2
POU3F1 / Lhx3	H14IG#E3	Hb9::hCD14-IRES-GFP	3, 4
POU3F1 / HOXA1	HC2G#H4	Hb9::hCD2GFP	1, 2
POU3F1 / Hoxa5	H14IG#E3	Hb9::hCD14-IRES-GFP	2, 3
POU3F1 / Hoxc6	H14IG#E3	Hb9::hCD14-IRES-GFP	1, 2
SFMBT2	HC2G#H4	Hb9::hCD2GFP	1, 2
Tag-RFP*	H14IG#E3	Hb9::hCD14-IRES-GFP	3, 4
TOX	HC2G#H4	Hb9::hCD2GFP	1, 2
Vwc2	HC2G#H4	Hb9::hCD2GFP	1, 2
YFP	HC2G#H4	Hb9::hCD2GFP	1, 2
YFP	H14IG#E3	Hb9::hCD14-IRES-GFP	1, 2
ZBTB7C	HC2G#H4	Hb9::hCD2GFP	1, 2
Zic1	HC2G#H4	Hb9::hCD2GFP	1, 2

Table S3. List of qPCR primer pairs. The primer sequences were obtained from PrimerBank (pga.mgh.harvard.edu/primerbank).

Download Table S3

Table S4. Complete list of all genes differentially expressed between sorted primary MNs of radial LMC, phrenic and non-phrenic C3-C5 identity.

Download Table S4

Table S5. List with the number of genes up- or down-regulated by induced candidate gene expression in ESC-MNs. The P-values were obtained using the Fisher test for overrepresentation of induced/repressed genes.

Download Table S5

Table S6. List of genes specific to primary phrenic neurons that are more than two-fold up- or down regulated by DOX-induced candidate determinants in ESC-MNs.

Download Table S6

Table S7. Complete list of all genes differentially regulated following DOX-induced expression of candidate genes in ESC-MNs.

Download Table S7

Table S8. Expression levels of selected candidate genes in iHoxa5, iNICD (10 hours), iPou3f1 and iPou3f1/Hoxa5 ESC-MNs as determined by qPCR. Gene expression in iYFP ESC-MNs was used as the baseline, and expression values are shown on a $\log_2$ scale. Two ESC-MNs populations derived from different ESC subclones were analysed for each genotype. The housekeeping genes Gapdh and Tbp were included as controls.

Download Table S8